Journal of Medicinal Chemistry

Article

pubs.acs.org/jmc

Design and Synthesis of Novel Lactate Dehydrogenase A Inhibitors by Fragment-Based Lead Generation†

Richard A. Ward,* Claire Brassington, Alexander L. Breeze, Alessandro Caputo, Susan Critchlow, Gareth Davies, Louise Goodwin, Giles Hassall, Ryan Greenwood, Geoffrey A. Holdgate, Michael Mrosek, Richard A. Norman, Stuart Pearson, Jonathan Tart, Julie A. Tucker, Martin Vogtherr,‡ David Whittaker, Jonathan Wingfield, Jon Winter, and Kevin Hudson

Oncology and Discovery Sciences iMEDs, AstraZeneca, Mereside, Alderley Park, Macclesfield, Cheshire, SK10 4TG, U.K.

Supporting Information

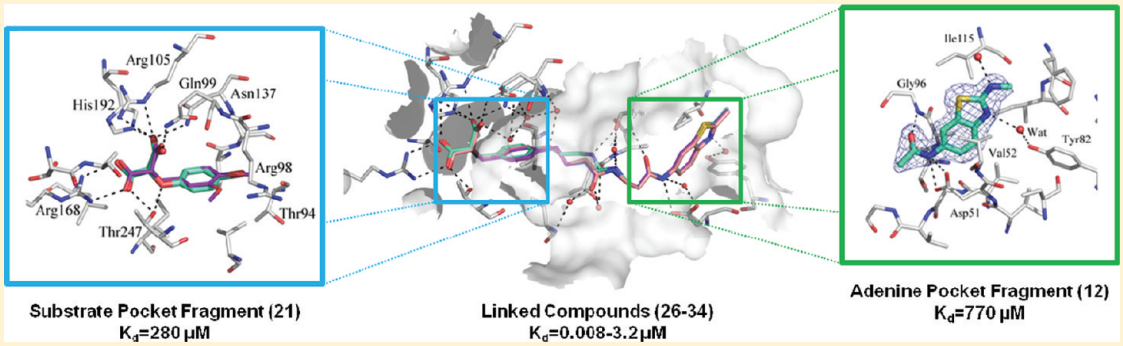

ABSTRACT: Lactate dehydrogenase A (LDHA) catalyzes the conversion of pyruvate to lactate, utilizing NADH as a cofactor. It has been identified as a potential therapeutic target in the area of cancer metabolism. In this manuscript we report our progress using fragment-based lead generation (FBLG), assisted by X-ray crystallography to develop small molecule LDHA inhibitors. Fragment hits were identified through NMR and SPR screening and optimized into lead compounds with nanomolar binding affinities via fragment linking. Also reported is their modification into cellular active compounds suitable for target validation work.

INTRODUCTION

In normal tissues, lactate generation is limited to anaerobic conditions where oxygen levels are low. In contrast, cancer cells preferentially convert glucose into lactate through glycolysis, even under normal oxygen concentrations, a phenomenon termed "aerobic glycolysis" or the Warburg effect.[1,2] Lactate dehydrogenase (LDH) is a tetrameric enzyme comprising subunits encoded by the LDHA and LDHB genes, which can be combined to generate five isoforms LDH1 (B4), LDH2 (B3A1), LDH3 (B2A2), LDH4 (B1A3), and LDH5 (A4). LDHA is a key glycolytic enzyme that catalyzes the formation of lactate from pyruvate, with LDHB favoring the backward conversion of pyruvate from lactate. LDHA is frequently up-regulated in clinical tumors, and high expression is often linked to poor prognosis.[3−7] In addition, inhibition of LDHA with siRNA or small molecules has been reported to induce oxidative stress and cell death.[8,9] In contrast, LDHB is located in heart muscle, which may indicate that achieving selectivity over this enzyme would be desirable. It is thus thought that LDHA could be a promising target for cancer therapy.

Our initial effort to identify inhibitors of LDHA utilized a high-throughput screen (HTS) of our corporate compound collection. Although active compounds were identified, the hit rate was relatively low at around 1%, when using a 30% inhibition cutoff with 10 μM compound concentration. These actives mainly grouped into small clusters or singletons. As a primary deconvolution tool for the HTS output, we measured the binding of compounds to purified recombinant human LDHA protein using ligand-observed (1D) NMR. We failed to confirm binding for any of the compounds tested; therefore, the actives of initial interest were considered likely to be false positives. One common mechanism for a significant number of the false positives was suspected to be inhibition of the target via silver, or other heavy metal impurities, in the compound samples.[10] This hypothesis was confirmed by the resynthesis of some compounds without the use of reagents containing silver. These examples were inactive upon testing. Although no way forward was identified from the HTS output, the ligand-observed NMR provided us with an assay suited for initiating a fragment-based lead generation (FBLG) campaign.[11,12] FBLG approaches have been particularly successful in a number of targets (including HSP90[13−16] and BACE[17−20]) and across the kinase target class more generally.[21] One of the most cited

Received: December 23, 2011
Published: March 14, 2012

dx.doi.org/10.1021/jm201734r | J. Med. Chem. 2012, 55, 3285−3306

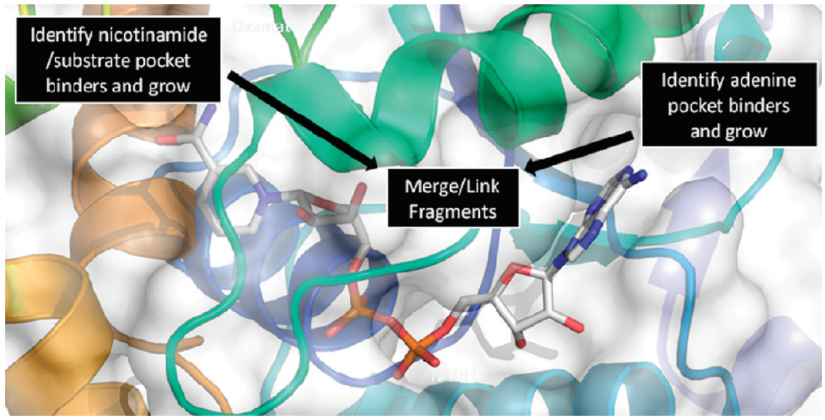

Figure 1. Summary of FBLG strategy to be applied to LDHA. X-ray crystal structure shown is PDB code 1i10.[25]

examples of this approach is the discovery of ABT-263, a potent inhibitor of Bcl-2, which has been reported by Abbott.[22] Our ligand-observed NMR capability provided an adequate throughput for the primary screening of fragments, and we developed a capability for follow-up confirmation and characterization using protein-observed (2D) NMR on stable isotope-labeled LDHA protein. However, measuring the binding affinity of compounds by protein-observed NMR was both time and resource intensive. It was apparent that a higher throughput assay would be required, so a number of label free approaches[23] to measure affinity were evaluated. After exploration of several options, the BIAcore assay[24] gave an acceptable balance of throughput, sensitivity, and data consistency. As part of the HTS workup, we had also established a soakable rat LDHA protein crystal structure system. Although a human LDHA protein crystal system has previously been published (PDB code 1i10[25]), we found the rat crystal system to be more amenable to soaking experiments and hypothesized that their high homology would make the rat system a suitable surrogate (Figure S1, Supporting Information). Human and rat LDHA sequences share 94% global sequence similarity using the Bestfit algorithm;[26] the cofactor and substrate binding sites, however, appear identical. We therefore prosecuted a FBLG campaign against LDHA, reasoning that the target may indeed be "druggable" or at least "ligandable"[27] but that our corporate collection might not contain compatible chemical matter. Analysis of the binding site of LDHA encouraged us that if we could find fragments binding to the different subpockets of the active site (i.e., adenine, nicotinamide, and substrate regions), then we could potentially link or merge multiple fragments (Figure 1). At this stage we also made the decision that we would not attempt to drive selectivity over LDHB, as the consequences of LDHB inhibition are not fully understood and it would significantly complicate the cascade of assays required. Sequence alignments between LDHA and LDHB, again using the BestFit algorithm, highlighted them to be 83% similar. However, the substrate and cofactor pockets show significantly higher levels of homology and the key catalytic residues are entirely conserved. Herein, we report the identification of fragment hits and their modification to produce cell active chemical probes.

RESULTS AND DISCUSSION

Assay Assessment. A survey of the literature identified a number of chemical probes to assess in our assays (NMR, BIAcore, and enzyme assay). Table 1 highlights compounds that were either synthesized or purchased and subsequently profiled in assays that could be used in an FBLG cascade.

Compound **1** has been described as an inhibitor of *Plasmodium falciparum* LDH with selectivity over human LDH and was synthesized using literature protocols.[28] This compound appears to be more active against human LDHB than LDHA (IC_{50} = 7.8 μM against LDHB compared with IC_{50} = 450 μM against LDHA), consistent with the literature precedent for competitive inhibition against lactate but not pyruvate.[28] The binding of this compound to LDHA was detected by NMR only when NADH or NAD^+ was also present in the assay. Weak binding (millimolar range) was observed in the presence of NADH, and tight (slow exchange) binding in the presence of 1 mM NAD^+, in agreement with the previously reported preference of the azole series for binding to the LDH−NAD^+ complex based on the results of kinetic analysis. The binding mode of this compound to the rat LDHA−NAD^+ complex was also confirmed by crystallography,[29] which shows it to bind in the substrate pocket in a manner similar to that previously reported for the binding of the equivalent oxadiazole to human LDHA−NAD^+ (PDB code 1t2f[28]). Although we were able to confirm binding and activity of compound **1**, we did not pursue this further, since compounds of this class show limited opportunity for further elaboration. Compounds **2**[30] and **3**[8] have been disclosed as LDHA inhibitors; however, we were unable to validate these compounds in our cascade as specific inhibitors. Compound **2** was synthesized using literature protocols[30] and showed significant superstoichiometric and nonspecific binding. Insufficient sample was available for testing in our enzyme assay. Compound **3** (known as FX-11) was also synthesized using the published protocols;[8] however, denaturation of the protein was observed in our assays and we were unable to generate a ligand bound crystal structure. Compound **4**[9] was synthesized using a modified version of the literature protocol (synthesis S1, Supporting Information). We were able to confirm specific binding of **4** to LDHA by 2D NMR; precipitation of protein−ligand complex at higher ligand concentrations hampered determination of an accurate K_d from the chemical shift titration data, but our calculated value of ~9 μM (which probably slightly underestimates the true K_d) is similar to the K_i of 8.9 μM against NADH reported by the authors. The pattern of LDHA backbone amide ^1H,^{15}N shifts induced by **4** indicated binding to the adenine subpocket of the cofactor site rather than the nicotinamide/substrate region as postulated by Granchi et al. BIAcore studies with compound **4** demonstrated significant levels of nonspecific binding.

dx.doi.org/10.1021/jm201734r | J. Med. Chem. 2012, 55, 3285−3306

Table 1. Data Generated on Published LDHA Inhibitors[a]

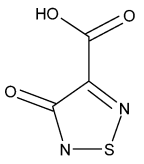

1

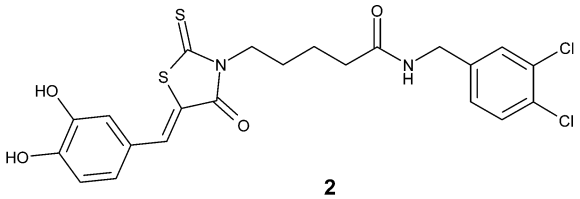

2

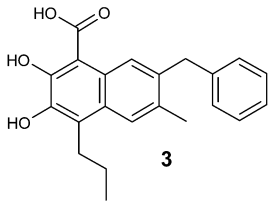

3

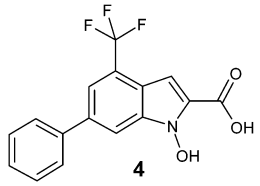

4

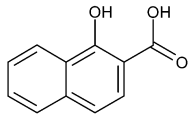

5

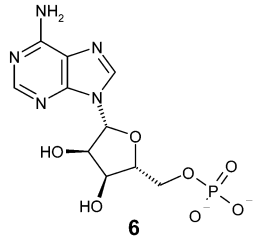

6

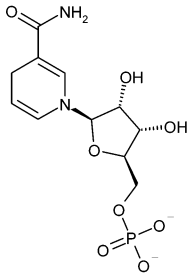

7

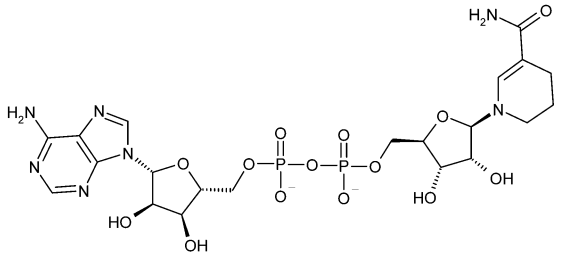

8

compd	K_d (μM)		IC_{50} (μM)	
	LDHA NMR	LDHA BIAcore	LDHA enzyme	LDHB enzyme
1	tight binding[b]	no binding	450	7.8
2	ambiguous	ambiguous	not tested	not tested
3	ambiguous	ambiguous	>500	not tested
4	>9.0[c]	ambiguous	>500	not tested
5	640	weak binding	>500	not tested
6	650	weak binding	>500	not tested
7	4000	weak binding	>500	not tested
8	tight binding	12.8	132	9.4

[a]Data quoted are an average of at least two independent measurements, apart from NMR data which were derived from a single experiment. [b]Measurement by NMR detected in the presence of 1 mM NAD^+. [c]K_d is a lower limit estimate from 2D chemical shift titration data and is influenced by poor solubility of protein/ligand complex.

Efforts to soak **4** into our rat LDHA crystal system identified electron density in the adenine pocket, but a binding mode could not be confirmed[29] and the compound showed no activity in our enzyme assay. Compounds containing the core structure of compound **5** have been previously disclosed as weak inhibitors of LDHA.[31] We were able to confirm binding by NMR and BIAcore, along with obtaining a crystal structure showing binding to the adenine pocket.[29] Compounds **4** and **5** therefore appear not to be potent or specific enough inhibitors of LDHA to show enzyme activity in our assay. Similarly, two fragments of NADH, compounds **6** and **7**, also show reproducible binding and yet were inactive in the enzyme assay. The key compound in validating our early cascade was compound **8** (tetrahydro-NAD[32]). Compound **8** showed tight binding by 2D NMR; it was therefore not possible to quantify the binding with a K_d value. Compound **8** also showed binding in BIAcore (12.8 μM) and was active in our enzyme assay with IC_{50} = 132 μM. This apparent drop-off in activity is likely due to the competition of

dx.doi.org/10.1021/jm201734r | J. Med. Chem. 2012, 55, 3285−3306

Table 2. Selected Examples from the Fragment Screen against LDHA[a]

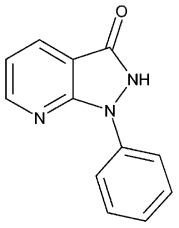

9

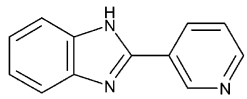

10

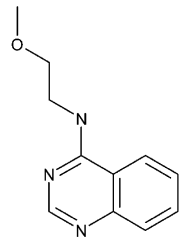

11

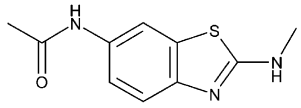

12

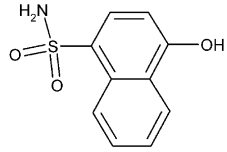

13

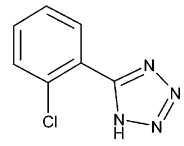

14

compd	LDHA NMR K_d (μM)	LE (NMR)	LDHA BIAcore K_d (μM)	LE (BIAcore)	LDHA enzyme IC_{50} (μM)
9	300	0.22	1600	0.16	>500
10	1400	0.19	weak binding		>500
11	2400	0.17	3000	0.17	>500
12	1000	0.20	770	0.17	>500
13	400	0.23	weak binding		>500
14	4200	0.20	weak binding		>500

[a]Data quoted are an average of at least two independent measurements, apart from NMR data which were derived from a single experiment.

the compounds with NADH in the enzyme assay compared to measuring their direct binding in BIACore. As observed for compound **1**, compound **8** also shows greater activity in our LDHB enzyme assay (IC_{50} = 9.4 μM) than in LDHA. These results obtained with **8** gave us confidence that were we to initiate a fragment screen to identify small molecules that bound tightly to the active site of LDHA and that were competitive with NADH, these could be a starting point for developing bona fide inhibitors.

Fragment Screening. Prior to the development of the BIAcore assay, ligand-observed NMR was used to screen our diverse library[12,33] of approximately 1000 fragments to identify chemical start points. Forty-four binders were identified (4.6% hit rate), which gave early encouragement that the target was indeed ligandable.[27] However, of the 27 hits prioritized for protein-observed NMR follow-up, we were only able to quantify binding for 13 fragments. Of these, only 3 fragments showed tighter binding than 1 mM with the range of affinities measured by NMR being from 300 to 4200 μM. The binding of a selection of these hits was measured in BIAcore to help further validate the assay, with a priority for follow-up given to fragments that showed consistent binding across both platforms. A selection of fragments from this initial screen are shown in Table 2, along with the NMR, BIAcore, and enzyme activity data where generated.

It became evident from this initial screen that the ligand efficiency (LE)[34] was generally modest, which reinforced how challenging it would be to develop potent small molecules against the target. In this manuscript, we have used the simplest measure of LE that is the pK_d divided by the number of heavy atoms. An additional observation was that although LE may be a suitable method for prioritizing fragments, the actual LE value varies depending on the assay, so comparing LE values across different assays may be misleading. For example, the most ligand efficient fragment according to NMR K_d data (**13**) did not have a measurable affinity by BIAcore, although weak binding was observed. This highlights the value of orthogonal assays in the context of FBLG. All fragment hits for which we obtained cocrystal structures with rat LDHA bound in the adenine pocket, which is a relatively shallow and open pocket. The binding modes of **12** and **14** to rat LDHA are shown in Figure 2 to highlight the interactions made by the fragments.

The asymmetric unit of the rat LDHA crystal system used in these studies contains a tetramer. In several cases, initial electron density for bound compound was clearly visible in only one of the four monomers, generally chain B. Unless indicated otherwise, all figures and discussions of binding mode refer to this monomer. The benzothiazole ring of **12** lies in the same hydrophobic pocket as that occupied by the adenine ring of NADH, between the side chains of Val-52 and Ile-115. Fragment **12** is additionally held in place via a water-mediated hydrogen bond between the thiazole nitrogen and the side chain hydroxyl of Tyr-82 and via extensive hydrogen bond interactions between the amide group and residues in the ribose binding site and at the mouth of the phosphate channel (amide NH to side chain carboxyl of Asp-51, and amide carbonyl to backbone NH and CO of Gly-96). The quality of the electron density indicates a degree of flexibility in the orientation of the *N*-methyl group which is directed toward solvent.

Fragment **14** binds in the same region as **12**, with the chlorophenyl group packed against the side chain of Val-52. The bound water previously observed in the complex with **12** has, however, been displaced, allowing the tetrazole to directly interact with the hydroxyl side chain of Tyr-82. The tetrazole ring of **14** extends into a region not occupied by **12**, where it may make a long-range interaction (>3.3 Å) with the side chain of Asn-122.

dx.doi.org/10.1021/jm201734r | J. Med. Chem. 2012, 55, 3285−3306

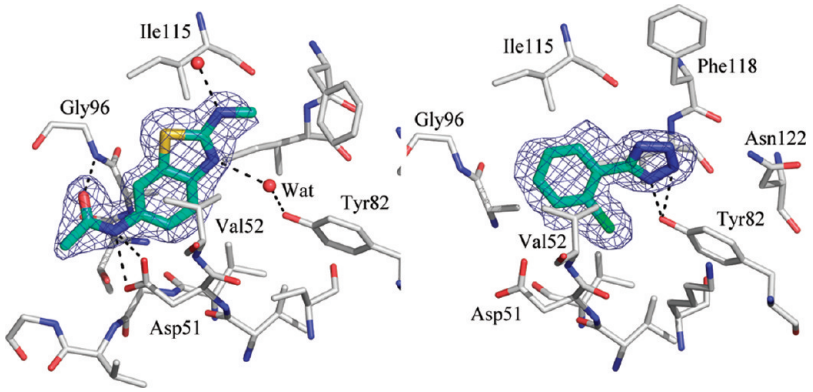

Figure 2. Binding mode of fragments **12** (left) and **14** (right) in the rat LDHA crystal structure, showing final $2F_o - F_c$ electron density for **12** and **14** (blue, 1.0σ level). Selected nearby water molecules and protein residues are shown. Hydrogen bonding interactions with the protein are indicated as dashed lines. All figures were prepared using PyMol.[35]

This binding mode is made possible by a flip of the Phe-118 side chain into an alternative rotamer. A number of fragments with acidic functionality, such as compound **14**, which we had expected to bind in the substrate pocket, were shown to occupy the adenine pocket upon soaking into rat LDHA crystals. The binding of acidic fragments in the adenine pocket had also been observed for compounds **4** and **5**, observations that were also supported by NMR data.

Our crystal system contains high concentrations of malonate (a substrate mimic), and this was observed to occupy the substrate binding site. We were therefore concerned that certain fragments with affinity for the substrate/nicotinamide pocket in solution might not be able to compete with endogenous malonate in the crystal system and thus were biased toward binding in the promiscuous adenine groove. We were unable to identify alternative crystallization conditions, most probably as a result of malonate binding at the substrate site and thus stabilizing the conformation of the flexible active site loop, and also binding to additional sites at the monomer interfaces and thus stabilizing the tetramer structure. Attempts to replace malonate with alternative precipitants in the buffers used for crystal soaking experiments showed citrate and sulfate to be compatible with maintenance of crystal integrity; however, the bound malonate at the substrate site was then replaced by citrate or sulfate.

We searched for analogues for a number of the confirmed fragment hits, focusing particularly on compounds **9**, **10**, **11**, and **12**. Of the hits we identified, these looked the most promising with respect to binding affinity, LE, and chemical feasibility. We had a concern with compound **13** in that it appeared to require the phenol group for the interaction with Tyr-82.[36] We believed the identification of a start point in the substrate pocket would potentially require an acidic fragment. We did not, therefore, wish to start with an acidic fragment (such as compound **14**) in the adenine pocket. The additional attraction of compounds such as **9**–**12** was that the crystal structures gave an indication of how the molecules could be grown toward the nictonamide region of the pocket. This helped focus analogue selection, as there appeared limited opportunities to pick up other interactions in the open adenine groove, although it does provide an opportunity to exploit the solvent exposed region of the pocket to modulate physicochemical properties. We initially identified a number of near-neighbors of each fragment from our corporate collection and commercial databases[37] for testing by NMR which then informed our wider testing using the higher throughput BIAcore assay. The NMR assay continued to be used in an orthogonal manner to confirm the binding of key compounds from BIAcore.

In total, around 350 analogues of the screening hits were tested in the BIAcore assay. The screening of these analogues initially investigated the effect of minor changes to the core scaffold and subsequently the effect of adding groups that might grow toward the nicotinamide pocket. A selection of analogues identified from these searches are shown in Table 3. Compound **15** was identified by looking for the minimal number of heavy atoms on the scaffold required to show binding in the BIAcore assay, which was an important parameter to establish with this technology now being the primary screening tool. Compound **16** contained a group with the potential to occupy the phosphate channel. No clear improvement in potency was observed, likely because of the phosphate channel being charged and solvent exposed.[38] Compound **17** provided the most notable increase in affinity, while maintaining the LE of compound **15**, through the addition of a lipophilic group. We were unable, however, to obtain an unambiguous binding mode for **17** in our rat LDHA crystal structure system. Compound **18** was subsequently tested in BIAcore, and although less potent than **17**, a complex crystal structure was successfully obtained (Figure 3).

The benzothiazole core of **18** binds identically to that of the parent fragment **12**, maintaining the water-mediated interaction between the thiazole nitrogen and the side chain hydroxyl of Tyr-82 and maintaining interactions through the amide group with the side chain of Asp-51 and the backbone of Gly-96. The carboxylic acid extends toward the phosphate binding region, picking up interactions with the side chain of Arg-98 and the backbone of Ala-29 (via water). Flexibility in the binding of this substituent is observed, as indicated by the poorer quality of the electron density for this region and variation in the modeled orientations between the four different molecules in the tetramer. The *S*-allyl substituent is not fully visible in the electron density, although its presence was confirmed by liquid chromatography–mass spectrometry (LC–MS) analysis of the samples used in the soaking experiment. The *S*-allyl has been modeled in a variety of conformations to reflect the disorder indicated by the lack of density while maintaining a preferred torsion angle around the S–CH_2 bond. Given the lack of density for the *S*-allyl substituent, the modest increase in potency observed for **18** (BIAcore K_d = 130 μM) compared

dx.doi.org/10.1021/jm201734r | *J. Med. Chem.* 2012, 55, 3285–3306

Table 3. Evolution of the Adenine Pocket Fragment 12 by Analogue Screening To Yield Compounds 17 and 18[a]

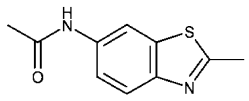

15

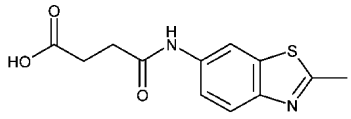

16

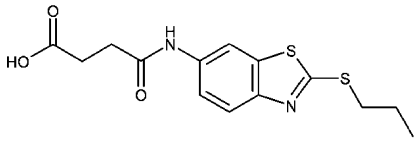

17

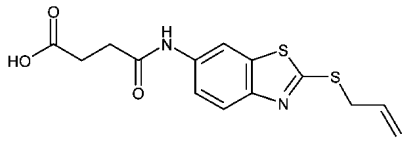

18

compd	LDHA BIAcore K_d (μM)	LE (BIAcore)	LDHA NMR K_d (μM)	LE (NMR)	LDHA enzyme IC_{50} (μM)
12	770	0.21	1000	0.2	>500
15	790	0.22	not tested		>500
16	500	0.16	540	0.18	>500
17	40	0.21	92	0.16	>500
18	130	0.l8	170	0.18	>500

[a]Data quoted are an average of at least two independent measurements, apart from NMR data which were derived from a single experiment.

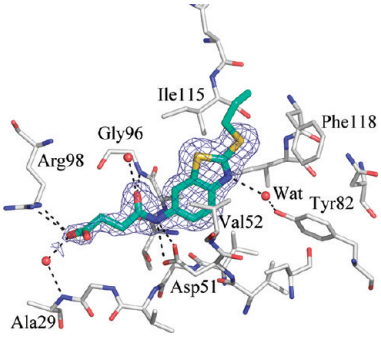

Figure 3. X-ray crystal structure of compound **18** bound in rat LDHA, showing final $2F_o - F_c$ electron density for **18** (blue, 1.0σ level). Selected nearby water molecules and protein residues are shown. Hydrogen bonding interactions with the protein are indicated as dashed lines.

with **16** (500 μM) is most likely driven by lipophilic interactions between the sulfur and Phe-118. In addition, we also monitored the ligand lipophilicity efficiency (LLE)[39−41] of our fragments, here defined as pK_d subtracted by cLogP (version 4.3). Although **15** and **17** have acceptable LE values (0.22 and 0.21, respectively), the LLE of the two compounds is relatively poor (0.83 and 0.64) reflecting the lipophilic nature of the adenine pocket. We were prepared to work with such fragments despite poor LLE, since we hypothesized that their relatively high lipophilicity would eventually be balanced out by a requirement for hydrophilic interactions in the substrate pocket. We also suspected that there would be scope to modulate properties through substitution at the solvent-exposed region of the adenine pocket. Our primary aim, therefore, was to find an "anchor" in the adenine pocket from which we could grow.

Targeting the Substrate Pocket. Having identified potential chemical start points bound in the adenine pocket, we turned our attention to fragments binding in the nicotinamide and/or substrate pockets. Results from the screening of our diverse fragment set indicated that finding hits for these pockets would be challenging, so we constructed a directed fragment set to target this region, exploiting a number of different data sources (Figure 4).

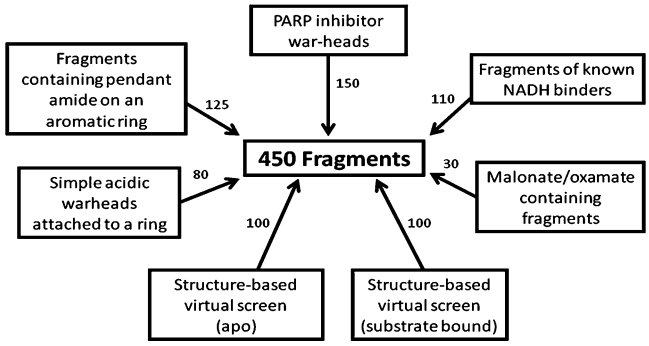

Figure 4. Summary of the combined nicotinamide/substrate pocket directed screening set.

One method used to identify potential fragments for screening was fragmentation of compounds described in the literature as NADH mimics, for example, inhibitors of targets such as poly-ADP-ribose polymerases (PARPs)[42,43] and nicotinamide phosphoribosyltransferase (NAMPRT).[44,45] Substructural searching was used to include fragments with a pendent amide directly attached to an aromatic ring as potential mimics of the key interaction of NADH in the nicotinamide pocket. To target the substrate pocket, we identified a set of acidic fragments through substructural searches, focusing on carboxylic acid groups directly attached to an aromatic or aliphatic five- or six-membered ring. Fragments of this type could target the substrate pocket in a similar manner as compound **1** and yet provide the potential for further elaboration. Furthermore, our in-house LDHA crystal structures showed malonate (**19**, Figure 5) binding in the substrate pocket. In contrast to oxamate, which is bound in a subset of published vertebrate LDH structures,[46−49] malonate provides a potential vector for further elaboration. Oxamate is a flat molecule, and it was less clear from inspection of the binding mode how this template could be exploited to grow out of the

dx.doi.org/10.1021/jm201734r | J. Med. Chem. 2012, 55, 3285−3306

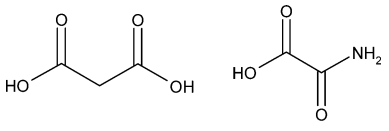

Figure 5. Chemical structure of malonate (**19**) and oxamate, present in the substrate pocket of in-house LDHA structures.

substrate pocket, similar to the situation reported for compound **1**. Malonate has the central methylene group as a potential growth point. We were able to detect the binding of malonate to LDHA by NMR with K_d = 5 mM, giving a respectable LE of 0.33. Fragments were therefore added to the screening set which contained malonate and oxamate substructures.

Finally, two protein-based virtual screens were performed using a published human muscle LDH structure, which has NADH and oxamate bound (PDB code 1i10[25]). In one of these virtual screens, both NADH and oxamate were removed (referred to as "apo"), while in the second only NADH was removed (referred to as "substrate bound"). Fragments were docked using Glide[50] in standard precision mode, with the top ranked hits visually assessed and prioritized for testing.

Considered fragments were also filtered by property and visual assessment. Although the use of rigid property-based cutoffs was avoided, the molecules generally conformed to a cLogP (version 4.3) between −1 and 3.5, fewer than 25 heavy atoms, 4 hydrogen bond donors, and 6 hydrogen bond acceptors with no structural alert flags from our in-house filtering protocol.[12] Exceptions to the filtering were made for compounds that were likely to be ionized or where there was a particularly strong rationale for inclusion, for example, compounds that were identified from multiple sources. In total, 695 fragments were identified by the above methods. However, there was significant overlap, leaving 450 unique fragments for testing.

The targeted screen was run at a single compound concentration of 2.5 mM using the BIAcore assay and identified 40 hits as clear binders (8.9% hit rate), with fragments being identified from all subsets. The majority of these initial hits, however, did not give reproducible K_d values in the BIAcore concentration response follow-up. Subsequent analysis showed that a significant proportion of these compounds also bound to acid-denatured LDHA, suggesting that their binding was nonspecific. A set of compounds showing binding only to folded LDHA were prioritized for crystallography, two examples of which are shown in Table 4.

A key result for the project was the identification of compounds **20** and **21**, which were selected because they contained the malonate substructure and also ranked favorably in the virtual screen against the "apo" structure. Compound **20** has improved affinity and LE compared to **21**; however, because **20** contains a bromine atom, LE can be misleading, as the increase in molecular weight and lipophilicity due to this single atom is large. This is highlighted if you compare their LLE values based on the BIAcore data, where **20** has a LLE of 2.1 while **21** has a more favorable LLE of 2.8. Compounds **20** and **21** were soaked into crystals of rat LDHA (Figure 6) and

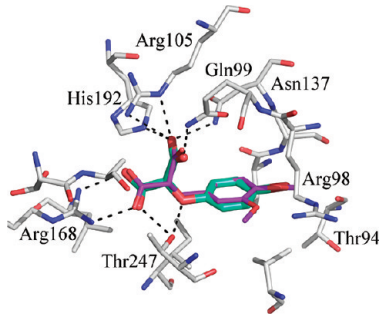

Figure 6. X-ray crystal structure of compound **20** (cyan) overlaid with **21** (purple), bound in the substrate pocket of LDHA. Selected protein residues are shown. Hydrogen bonding interactions with the protein are indicated as dashed lines.

shown to bind in such a way as to occupy both the substrate and nicotinamide pockets.

Compounds **20** and **21** bridge the nicotinamide and substrate pockets with the diacid binding in the substrate pocket in a manner similar to that observed for malonate alone. The 4-bromobenzyl and 3,4-dimethoxybenzyl groups overlap with the area occupied by the nicotinamide ring, placing the 4-substituent where the oxygen of the ribose ring would otherwise be located. The oxygen atoms of the diacid moiety are involved in polar interactions with the side chains of residues lining the substrate binding pocket: Arg-105, Asn-137, Arg-168, His-192, and Thr-247 and in chains B and C, Gln-99. The linker oxygen of **20** contacts the side chain of Thr-247, while a flip at the prochiral central carbon of the diacid group in **21** shifts the equivalent carbon ~0.6 Å away from Thr-247. This movement results in a subtle shift of the benzyl ring overlaying the methyl group of the *p*-methoxy substituent in **21** onto the position occupied by the *p*-bromo of **20**. These two groups are then oriented such that they may form polar

Table 4. Selected Hits from Output of Directed Fragment Screening against the Nicotinamide/Substrate Pocket[a]

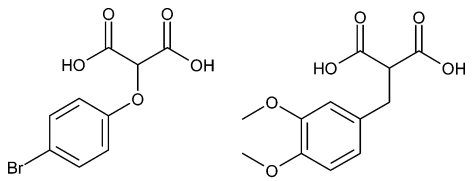

compd	LDHA BIAcore K_d (μM)	LE (BIAcore)	LDHA NMR K_d (μM)	LE (NMR)	LDHA enzyme IC_{50} (μM)
20	210	0.24	470	0.22	>500
21	280	0.20	1000	0.17	>500

[a]Data quoted are an average of at least two independent measurements, apart from NMR data which were derived from a single experiment.

dx.doi.org/10.1021/jm201734r | J. Med. Chem. 2012, 55, 3285−3306

interactions with the backbone carbonyl of Thr-94. The *m*-methoxy substituent of **21** is relatively solvent exposed.

Inspection of the complex structures indicates that removal of the bromine atom in **20** would be required to allow growth along the phosphate channel. We were therefore encouraged by the data on compound **21**, in which the para substituent is a methoxy group, potentially offering such a growth opportunity. Only a limited number of analogues could subsequently be tested in the BIAcore assay, because of the relative scarcity of the malonate "warhead" in our corporate collection. A small set of fragments related to compounds **20** and **21** from which one of the acidic groups had been removed or replaced were tested; however, the binding affinity was too low for reliable detection of binding for these compounds. We were aware that the diacidic nature of the malonate motif would cause significant challenges in terms of cell membrane permeability and ADME properties,[51] despite providing a tight binding chemical start point in the substrate pocket. We took the decision to retain the diacid until we had built additional potency elsewhere in the molecule, at which point we would be in a better position to assess the full impact of modifying or removing one of the acidic functionalities.

Fragment Growing. An overlay of the structures of compounds **12** and **20** in complex with rat LDHA (Figure 7) showed

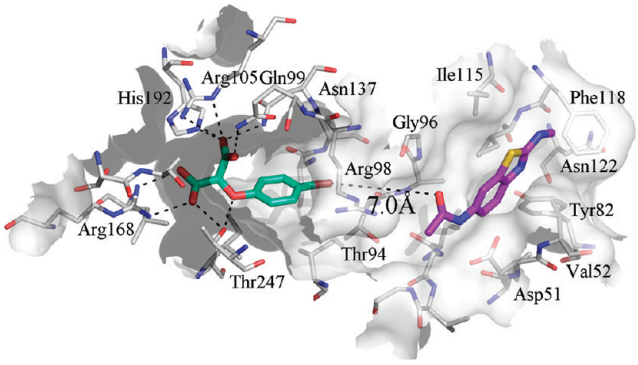

Figure 7. Overlay of the complex structures of compounds **12** (purple) and **20** (cyan) with rat LDHA, showing the shortest distance separating the fragments.

that they were separated by a significant distance (over 7 Å) that would need to be reduced before we could consider linking. Compound **18** extends toward the phosphate channel, but it does not close the overall gap between the two fragments (Figure S2, Supporting Information) and the substituent directed toward the nicotinamide pocket already contains an acidic group, which would need to be removed or modified to allow further growth.

Having exhausted all the relevant analogues from our corporate collection, we took the decision to synthesize compounds in order to grow the fragments toward each other. To achieve this aim, we synthesized sets of compounds growing from the adenine pocket (**A1** and **A2**, Scheme 1) and from the substrate pocket, **S1** and **S2** (Schemes 2 and 3).

Scheme 2. Synthesis of Substrate Targeted Library S1[a]

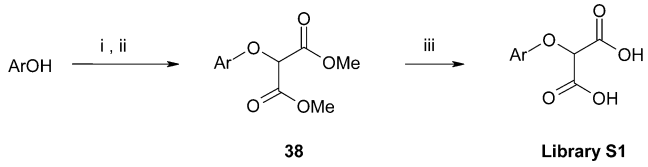

[a](i) NaOMe, MeOH, rt; (ii) diethyl 2-chloromalonate, 70 °C, 1−3 days; (iii) LiOH, THF, water, rt, 16 h.

We did not expect to make significant increases in potency in this growing stage, as the phosphate pocket is highly solvent exposed and charged. Our aim was to maintain ligand efficiency where possible and to close the distance between the fragments. Amide couplings provided compounds for libraries **A1** and **A2** from the previously reported[52] aminobenzothiazole **36** and commercially available compound **37**.

Libraries **S1** and **S2** were accessed from the corresponding substituted phenols, benzaldehydes, or benzyl halides. Niederl and Roth[53] reported the alkylation of sodium phenolates with halomalonate esters. In accordance with their findings, we found that use of diethyl 2-chloromalonate was optimal, as it gave exclusively monophenoxymalonates **38** (Scheme 2), although reaction was usually incomplete, especially for electron rich phenols. The more reactive diethyl 2-bromomalonate led to formation of diphenoxymalonates via self-bromination. We obtained products from a diverse range of phenols but found that hydroxy heterocycles and aliphatic alcohols were unsuccessful. Hydrolysis under basic conditions subsequently gave the library **S1** diacids. Because of intramolecular H-bonding, the first hydrolysis to the monoacid was significantly faster (reaction time of ∼30 min at ambient temperature) than the second hydrolysis (reaction time of ∼2 days).

Knoevenagel condensation of aromatic aldehydes and malonate esters has been reported[54] catalyzed by amine tipped dendrimers (Scheme 3). We found that polymer-supported trisamine resin together with molecular sieves was also effective

Scheme 1. Synthesis of Adenine Pocket Libraries[a]

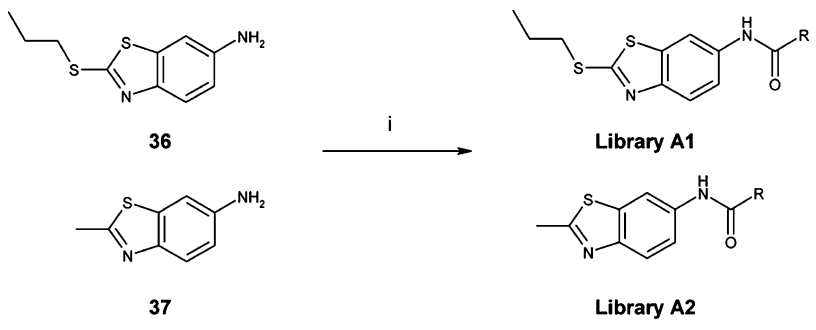

[a](i) RCO_2H, HATU, DIPEA, DMF, rt, 16 h.

dx.doi.org/10.1021/jm201734r | J. Med. Chem. 2012, 55, 3285−3306

Scheme 3. Synthesis of Substrate Targeted Library S2[a]

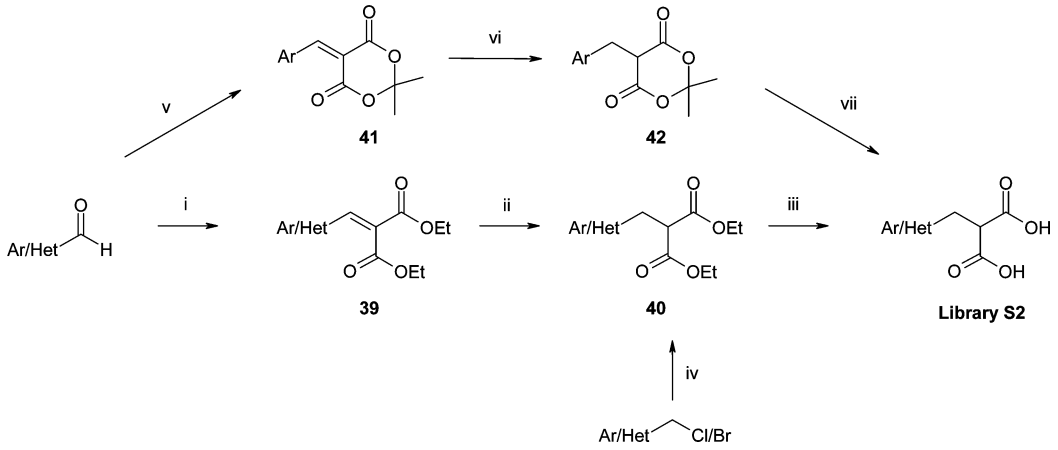

[a](i) Diethyl malonate, PS-trisamine, 4 Å molecular sieves, EtOH, 50 °C, 1−3 days; (ii) H_2, Pd−C, EtOH; (iii) LiOH, water, THF, rt, 16 h; (iv) diethyl malonate, NaH, THF; (v) Meldrum's acid, H_2O, 70 °C, 4 h; (vi) $NaBH_4$, AcOH, DCM, rt, 1 h; (vii) LiOH, H_2O, 120 °C, 1.5 h.

as a catalyst for this reaction. This gave good results on a number of substrates, with the advantage that the catalyst could be removed by filtration. Especially in the case of electron-deficient aldehydes, the temperature and number of equivalents of malonate must be carefully controlled to avoid the further, irreversible reaction of the alkylidene products **39** with excess malonate. Catalytic hydrogenation gave alkyl malonates **40**, which were hydrolyzed to afford malonic acids for library **S2**.

Another approach to these compounds was developed via alkyl-substituted Meldrum's acids. Benzaldehydes were condensed with Meldrum's acid under the aqueous, uncatalyzed conditions of Bigi[55] to yield the alkylidines **41**. Reduction to the alkyl derivatives **42** was effected with $NaBH_4$/AcOH, followed by basic hydrolysis to the malonic acids. Where Knoevenagel synthesis was not feasible, alkyl malonates **40** were formed via alkylation of diethyl malonate. Dialkylation was unavoidable, but the required materials could be separated by chromatography.

The libraries based on the template **S1** were less chemically tractable than for **S2**. The final hydrolysis step often led to partial cleavage of the C−O bond to the malonate position.

For libraries **A1** and **A2**, protein−ligand docking was used to focus the selection of a set of commercially available reagents to groups that grew in the preferred direction; however, as we were not confident that the binding mode prediction (or scoring) would be reliable in this region of the protein, it was used as a method of prioritization, as opposed to rigid filtering. An issue we quickly identified when synthesizing library **A1** was the relatively poor solubility of these compounds, which prevented us from measuring accurate K_d values for many of these molecules. The decision was taken to abandon library **A1** and switch the scaffold to the less lipophilic and more soluble library scaffold **A2**, keeping the substituents the same. This change, however, decreased the affinity of the library template by around an order of magnitude, comparing compounds **16** (K_d of 500 μM by NMR) against **17** (40 μM). As part of our exploitation of template **A2**, we synthesized approximately 150 compounds.

BIAcore measurements highlighted 10 compounds from library **A2** that showed an improved (or at least broadly consistent) affinity over the early compounds based on the same template. All of these compounds were soaked into rat LDHA crystals in order to determine the orientation of the substituent on the amide. Compounds for which structures were obtained were bound with the benzothiazole core in the same position as the parent fragment, **15**; however, out of all the amide side chains, only the urea group in **22** (Table 5) was directed toward the phosphate channel. Although no more potent than compound **15**, compound **22** was identified as an attractive hit, as the urea group made specific interactions with the protein that appeared to "cut the corner" of the NADH binding mode, thereby avoiding the charged phosphate pocket and bringing our fragments within 3.5 Å at closest approach (Figure 8). The compound also offered clear opportunities for further growth and optimization.

The benzothiazole core of **22** binds in the adenine pocket as described previously for **12** and **18**, while the urea group extends into the phosphate channel, where it is anchored by multiple direct and water-mediated interactions. The amino groups make a bidentate interaction with the backbone carbonyl of Gly-96, while the urea carbonyl makes water mediated contacts to Gly-28, Ala-29, Val-30 and Gly-31 (backbone NH), and Thr-94 (side chain hydroxyl). Dual soaks with **20** plus **22** or with **21** plus **22** confirmed that both fragments could bind simultaneously and that the binding modes were not perturbed (Figure S3, Supporting Information).

We targeted an immediate increase in potency by modifying compound **22** with the *S*-propyl group to give compound **23** (Table 5), in the hope that it might allow us to observe enzyme activity, helping us to further validate our approach. A significant increase in affinity was observed in the BIAcore assay (K_d = 35 μM for **23** compared with K_d = 770 μM for **22**), consistent with previous SAR; however, this appeared not to be sufficient to result in measurable enzyme activity. Compound **24** was synthesized to confirm the hypothesis derived from visual analysis of the crystal structure that the urea group could be further substituted to grow into the nicotinamide pocket. Encouragingly, when the BIAcore data for **24** were compared to **22** (K_d = 160 μM versus K_d = 770 μM) a modest improvement in LE from 0.16 to 0.18 was observed, indicating further growth is tolerated. The complex crystal structure showed an identical binding mode for **24** and **22** (Figure S4, Supporting Information).

Seventy compounds were synthesized across templates **S1** and **S2**. Analysis of the crystal structures of compounds **20** and **21** in complex with rat LDHA resulted in meta- or para-substituents being prioritized in order to grow the fragments

dx.doi.org/10.1021/jm201734r | J. Med. Chem. 2012, 55, 3285−3306

Table 5. Selected Binders from the Adenine and Substrate Pocket Libraries[a]

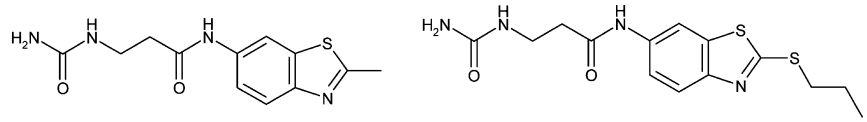

22

23

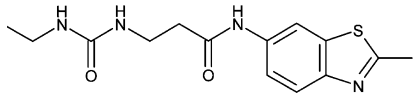

24

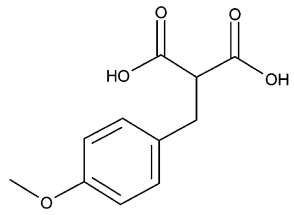

25

compd	LDHA BIAcore K_d (μM)	LE (BIAcore)	LDHA NMR K_d (μM)	LE (NMR)	LDHA enzyme IC_{50} (μM)
15	790	0.22	not tested		>500
22	770	0.16	binding		>500
23	35	0.20	binding		>500
24	160	0.18	not tested		>500
25	1100	0.18	240	0.23	>500

[a]Data quoted are an average of at least two independent measurements, apart from NMR data which were derived from a single experiment.

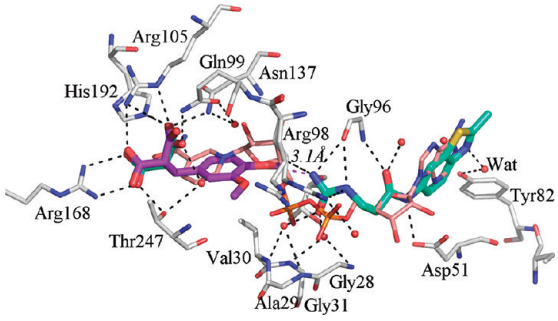

Figure 8. Binding mode of compound **21** (purple), superimposed with the crystal structure of fragment **22** (cyan) and the NADH bound 1i10[25] structure (pink).

along the phosphate channel toward the adenine pocket. We included substituents such as methoxy, amides, sulfonamides, and amines to provide additional growth points should the group be tolerated by the protein. The libraries based on the template **S2** were both more chemically tractable than those for **S1** and consistently showed an improved affinity, resulting in us favoring the carbon-linked malonate template. Compound **25** (Table 5) was one of the most interesting examples, with K_d = 1100 μM. This compound was designed to assess whether the *p*-methoxy functionality in **21** could be used as a growth vector. Compound **25** also showed binding by NMR, with K_d = 240 μM.

Fragment Linking. With the gap between the two fragments now reduced to less than 3 Å (Figure S4, Supporting Information), we decided to link the two molecules **24** and **25**. We used the crystal structure of compound **21** to inform us of the likely binding mode of **25**, as the crystal structure of **25** was not available at the time. Multistep chemistry routes meant that we required a strong rationale for making specific linked compounds. Possible target compounds with a range of linkers were modeled in the active site of LDHA with input from medicinal, structural, and synthetic chemists. The effect of the linker on the position of the individual fragments was monitored computationally, along with the agreement of the linker geometry with experimental data in the Cambridge Structural Database[56] (CSD). Compound **26** was the first linked compound (represented by core 1) made as a one-off compound to test our hypothesis. Gratifyingly, **26** produced a breakthrough increase in affinity (K_d = 0.13 μM) while maintaining LE (Table 6).

The synthesis of linked compounds required substrate and adenine pocket fragments containing pendent amine groups. To access the malonate-bearing fragment for core 1 (Scheme 4), aldehyde **43** was formed by Mitsunobu coupling of 4-hydroxybenzaldehyde and *N*-Boc-aminoethanol. **43** was subjected to our previous Knoevenagel conditions; subsequent hydrogenation of the alkylidine product **44** led to malonate **45**. Treatment of **45** with HCl under anhydrous condtions removed the Boc group to give **46** while leaving the malonate esters intact. We found that **46** in free-base form was unstable to polymerization on storage; it was either formed and used immediately or stored in salt form.

The adenine pocket unit was formed via amide coupling of **37** and acid **47** (Scheme 5). The resulting amide **48** was deprotected with TFA to give **49**. Our initial strategy for constructing the urea linker was via the active phenyl carbamate **50** (Scheme 6), which was reacted with the malonate-bearing amine **46** to afford the fully linked molecule **51**. Basic ester hydrolysis afforded the final compound **26**.

Core 2 required building block **59**, which involved a longer route (Scheme 7). Boc protection of commercially available amino acid salt **52** followed by esterification gave **53**, which was converted to aldehyde **55** via alcohol **54**. The Knoevenagel reaction of **55** was problematic; the alkylidine malonate product **56** was prone to reaction with a second equivalent of malonate to give **57**. This occurred more readily than for core 1 analogue **44**; in that case the *p*-oxygen presumably moderated the electrophilicity of the aldehyde carbon. Formation of impurity **57** was irreversible, and it could not be separated

dx.doi.org/10.1021/jm201734r | *J. Med. Chem.* 2012, 55, 3285−3306

Table 6. BIAcore and Enzyme Activity Data on Linked Compounds[a]

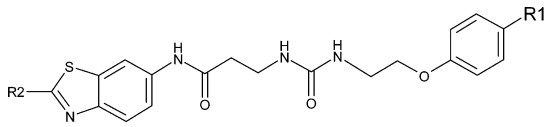

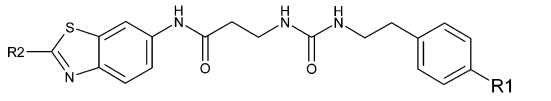

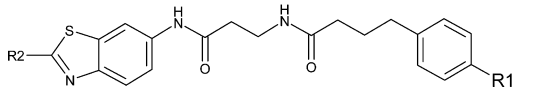

Compound ID	Core	R1	R2	LDHA BIAcore K_d (μM)	LE (BIAcore)	LDHA Enzyme IC_{50} (μM)
26	1	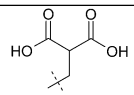	Me	0.13	0.19	4.2
27	1	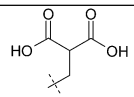	*S*-propyl	0.046	0.19	3.1
28	1	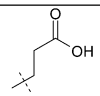	Me	3.2	0.17	86.2
29	2	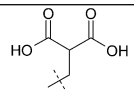	Me	0.069	0.20	1.9
30	2	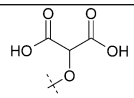	Me	1.2	0.17	29.5
31	2	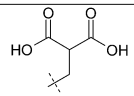	*S*-propyl	0.06	0.19	0.29
32	2	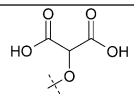	*S*-propyl	0.180	0.18	7.4
33	3	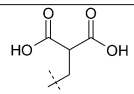	Me	0.093	0.20	0.5
34	3	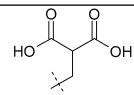	*S*-propyl	0.008	0.21	0.27

[a]Data quoted are an average of at least two independent measurements.

from **56** by chromatography. It could be controlled by reducing the excess of malonate used in the reaction; however, this led to incomplete reactions and lower yields. Our best solution was to take this inseparable mixture of product and starting material through to the subsequent hydrogenation step. Any remaining **55** was reduced to the corresponding toluene derivative which could then be removed from product **58** by chromatography. Finally, acidic deprotection of the Boc group gave the required amine **59**. This compound was even more prone to polymerization than **46** and was also used immediately or stored in salt form.

The starting point for the oxymalonate linked compounds was 4-hydroxyphenethylamine. Reaction with phenyl chloroformate under aqueous basic conditions gave clean conversion to the active carbamate **60** (Scheme 8). Coupling with amine **49** gave the linked phenol **61** which was able to displace

dx.doi.org/10.1021/jm201734r | *J. Med. Chem.* 2012, 55, 3285−3306

Scheme 4. Synthesis of Substrate Template for Core 1 Fragment Linking[a]

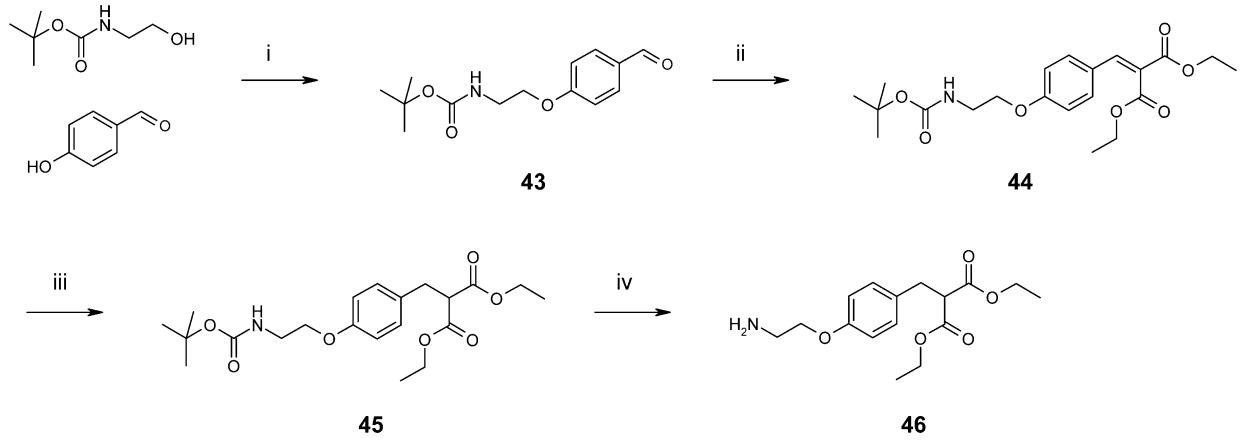

[a](i) DIAD, PPh_3, THF; (ii) diethyl malonate, PS-trisamine, 4 Å molecular sieves, EtOH, 50 °C, 80%; (iii) H_2,Pd−C, EtOH, rt, 16 h, 95%; (iv) TFA, DCM, rt, 16 h, 99%.

Scheme 5. Synthesis of Adenine Template for Fragment Linking[a]

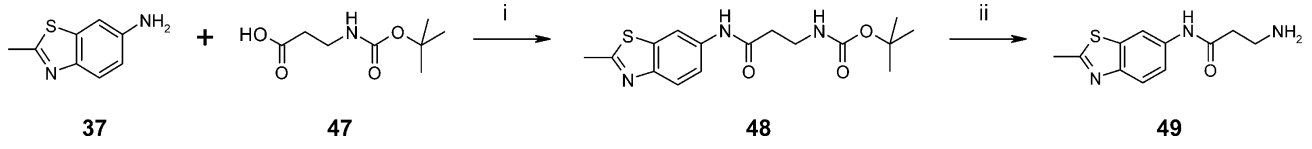

[a](i) HATU, DIPEA, DMF, rt, 16 h, 99%; (ii) TFA, DCM, 18 h, 93%.

Scheme 6. Fragment Linking of Core 1 Compounds[a]

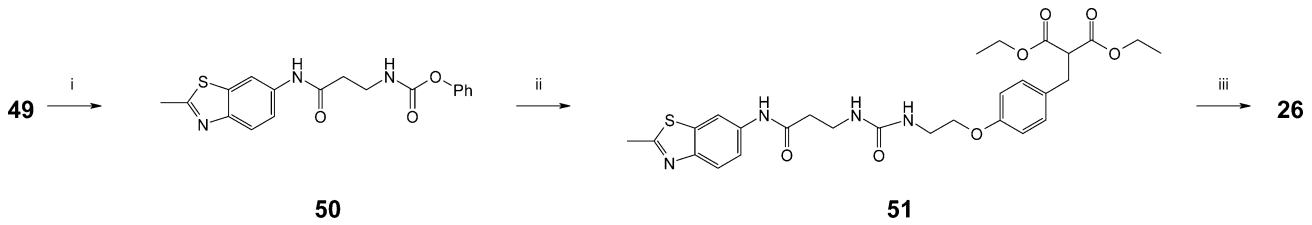

[a](i) Phenyl chloroformate, pyridine, THF, 0 °C to rt, 16 h, 39%; (ii) amine **46**, NMP, rt, 3 days, 53%; (iii) $LiOH·H_2O$, H_2O, EtOH, rt, 2 days, 48%.

dimethyl 2-chloromalonate under basic conditions to give oxymalonate diester **62**. Hydrolysis to **63** was much quicker than for core 2 because of the electron-withdrawing effect of the oxygen. The reactions had to be stopped quickly after completion, as prolonged exposure to base led to cleavage of the malonate group.

Some of our urea-linked compounds, such as **27** and **32**, were synthesized via the phenyl carbamates of the malonate-bearing amines **46** and **59**; however, we encountered lower yields, having issues with homocoupling and the formation of byproduct. An improved linking approach was developed for the synthesis of subsequent urea-linked molecules, for example, **29** (Scheme 9). Reaction of amine **49** with 1 equiv of *N*,*N*′-carbonyldiimidazole (CDI) gave the active intermediate **64** as a stable solid which could be stored. This was reacted with the malonate-bearing amine **59** to give, after subsequent hydrolysis, compound **29** cleanly and in good yield.

The acid **70** required for core 3 was synthesized starting from 4-phenylbutanoic acid (Scheme 10) and was converted to the ethyl ester **65** under acid catalysis. Duff reaction with hexamethylenetetramine introduced the aldehyde group selectively into the 4-position to give **66** in 31% yield (lit. 57%).[57] An orthogonal protecting group strategy was needed, so the ethyl ester **66** was converted to the corresponding benzyl ester **68** via acid **67**. The malonate ester moiety was connected via Knoevenagel condensation as previously. As with **56**, overreaction forming the bis-malonate adduct was a serious issue in the synthesis of **69**, so yields were generally low. Hydrogenation accomplished simultaneous reduction of the double bond and removal of the benzyl group to give **70**. This was a relatively stable compound, although air oxidation to acid was observed in some of the preceding aldehyde-bearing intermediates.

The linked compound **71** was formed by a simple amide coupling to amine **49** (Scheme 11). With no vulnerable groups in the molecule, hydrolysis to **33** was straightforward.

An enzyme-complexed structure of **26** was obtained using the rat LDHA crystal system (Figure 9a). This confirmed the binding mode predicted using the structures of the two separate fragments (**21** and **24**) and modeling work on the linker region. In agreement with our earlier structural data for **21** and **24**, the linking group appeared to take a more direct route through the phosphate channel than is the case for NADH (Figure 9b), thereby both avoiding the need for a phosphate isostere and minimizing molecular size. The potency gained from joining fragments **24** (K_d = 160 μM)

dx.doi.org/10.1021/jm201734r | J. Med. Chem. 2012, 55, 3285−3306

Scheme 7. Synthesis of Substrate Template for Carbon-Linked Core 2 Compounds[a]

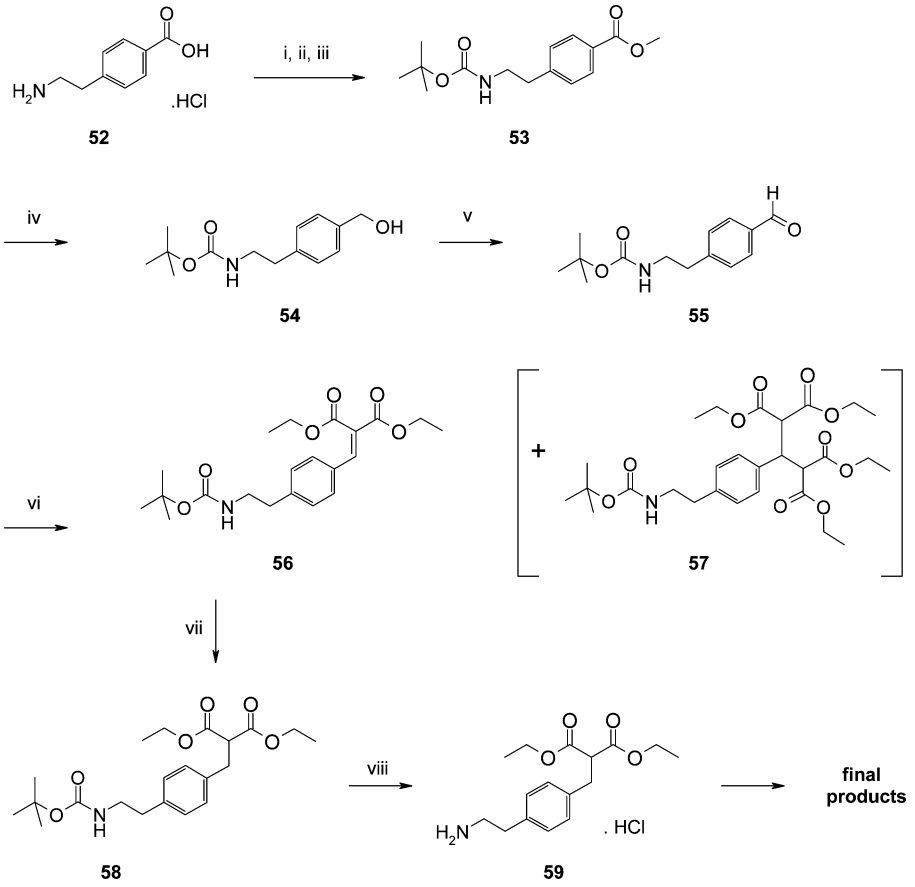

[a](i) Boc_2O, NaOH, EtOH, H_2O, rt, 3 days, 43%; (ii) CDI, DCM, rt, 2 h; (iii) MeOH, rt, 16 h, 84% (two steps); (iv) $LiAlH_4$, THF, 0 °C, 2 h, 99%; (v) MnO_2, DCM, rt, 4 days, 88%; (vi) diethyl malonate, PS-trisamine, 4 Å molecular sieves, EtOH, 60 °C, 16 h, 33%; (vii) H_2, 5% Pd–C, EtOH, rt, 16 h, 75%; (viii) HCl in 1,4-dioxane, DCM, rt, 16 h, quant.

Scheme 8. Synthesis of Substrate Template for Oxygen-Linked Core 2 Compounds[a]

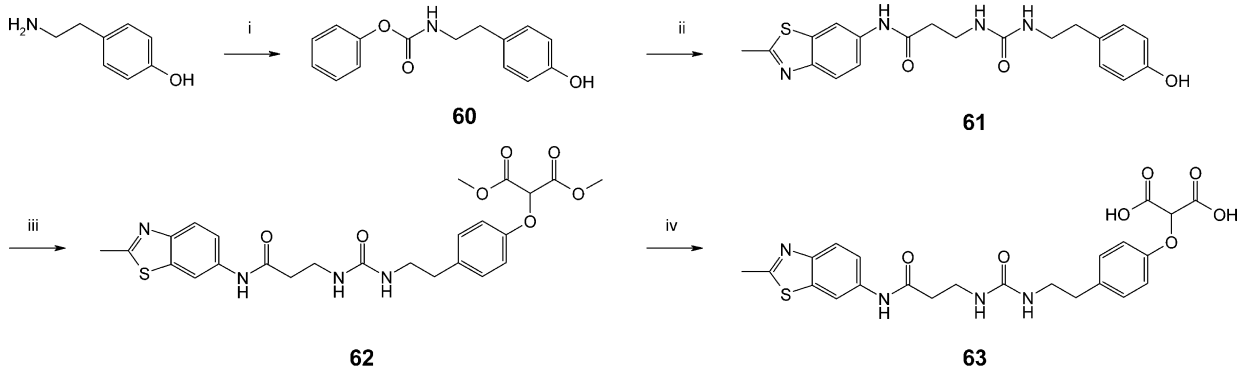

[a](i) Phenyl chloroformate, $NaHCO_3$, 1,4-dioxane, water, 4 h, quant; (ii) amine **49**, NMP, 70 °C, 24 h, 56%; (iii) dimethyl 2-chloromalonate, K_2CO_3, DMF, rt, 2 days, 28%; (iv) NaOH, H_2O, THF, rt, 20 min, 79%.

and **25** (1100 μM) into a linked molecule with K_d = 0.13 μM (**26**) was over 3 orders of magnitude. Critically, for this linking process the LE is broadly maintained at 0.19. There are limited examples in the literature where fragment linking has given improvements of, or even maintained, the ligand efficiency of the initial fragments,[58−63] highlighting the challenges inherent in this approach.

Apart from tetrahydro-NAD (**8**), compound **26** was the first compound synthesized that showed activity in our enzyme assay and was immediately optimized by exploiting our prior knowledge of SAR to replace the methyl on the benzothiazole with an *S*-propyl to give compound **27**. This resulted in a ∼3-fold improvement in affinity as measured by BIACore. Compound **28** was made to probe the impact of removing one of the carboxylic acids from a linked compound. We observed a decrease in affinity of more than an order of magnitude compared to **26** (K_d = 3.2 μM for **28** versus K_d = 0.13 μM for **26**) along with a reduction in LE.

dx.doi.org/10.1021/jm201734r | J. Med. Chem. 2012, 55, 3285−3306

Scheme 9. Improved Method for Fragment Linking of Carbon-Linked Core 2 Compounds[a]

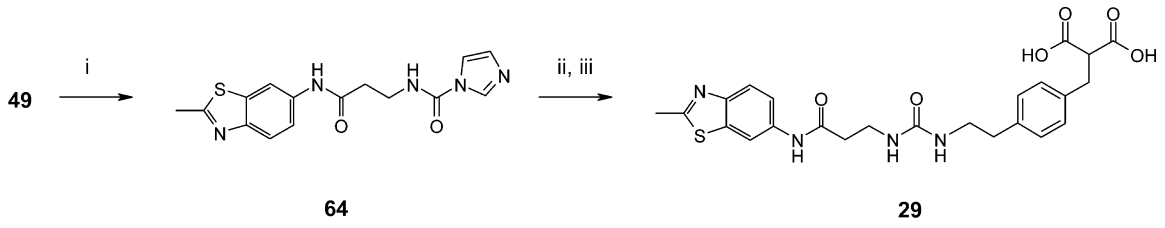

[a](i) 1,1-carbonyl diimidazole, DCM, rt, 2 h, 60%; (ii) amine **59**·HCl, NMP, 24 h, 56%; (iii) NaOH, H_2O, rt, 2 days, 76%.

Scheme 10. Synthesisis of Substrate Template for Core 3 Fragment Linking[a]

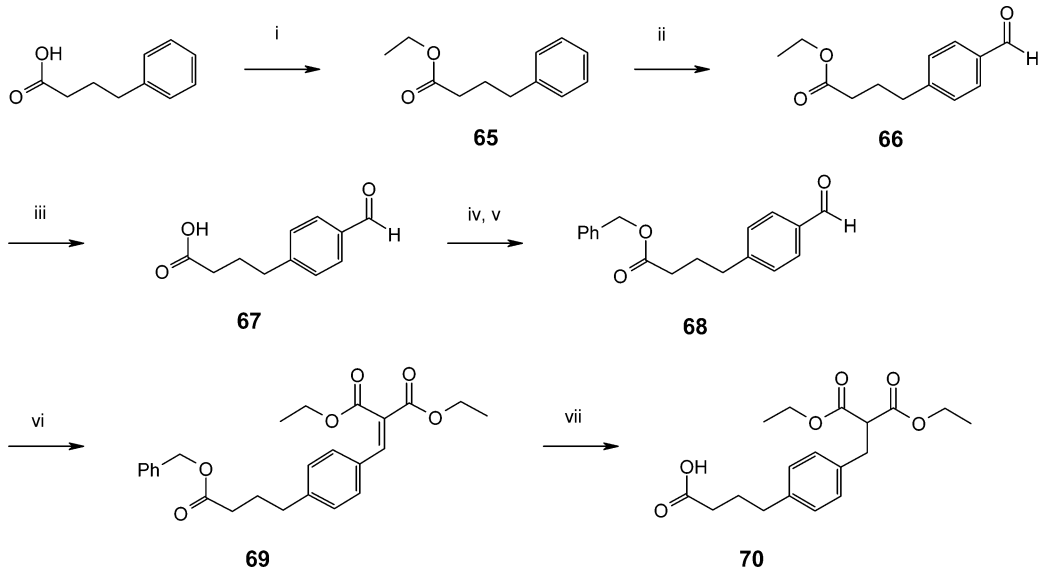

[a](i) conc H_2SO_4, EtOH, reflux, 20 h, quant; (ii) hexamethylenetetramine, TFA, reflux, 16 h, 31%; (iii) LiOH·H_2O, THF, water, rt, 16 h, 91%; (iv) CDI, imidazole, rt, 3 h; (v) BnOH, rt, 16 h, 81% (two steps); (vi) diethyl malonate, PS-trisamine, 4 Å molecular sieves, toluene, reflux, 3 days, 54%; (vii) H_2, 5% Pd−C, EtOAc, rt, 16 h, quant.

Scheme 11. Fragment Linking of Core 3 Compounds[a]

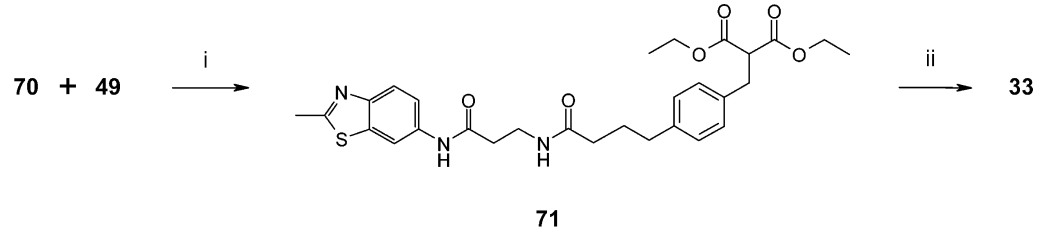

[a](i) HATU, DIPEA, DMF, rt, 16 h, 61%; (ii) NaOH, H_2O, EtOH, rt, 2 days, 79%.

We subsequently made a number of other linker groups in our search for improved affinity and LE and to broaden our knowledge of the SAR. Core 2, with a shorter linking group, looked particularly promising from a modeling perspective. The BIAcore data showed a modest improvement in binding affinity for one of the core 2 equivalents made (K_d = 0.13 μM for **26** compared with K_d = 0.069 μM for **29**), although the binding affinity of the second pair, compounds **27** (K_d = 0.046 μM) and **31** (K_d = 0.06 μM), remained broadly unchanged. However, core 2 compounds **29** and **31** had improved enzyme activity over their core 1 equivalents (**26** and **27**, respectively). Core 3 was made to assess the impact of replacing a nitrogen of the urea with carbon, converting the group into an amide. This resulted in a further increase in potency when compared with core 1 (compounds **33** and **34**). Compound **34** was both the most tightly binding compound by BIAcore (K_d = 0.008 μM) and the most potent compound in the enzyme assay (IC_{50} = 0.27 μM).

Across the data set in Table 6, replacement of methyl with *S*-propyl gave a clear increase in the binding affinity in two of the three matched pairs (**26** compared with **27** and **33** compared with **34**) with LE in general maintained. For the third pair (**29** and **31**) although binding affinity is largely unchanged, compound **31** (IC_{50} = 0.29 μM) was more potent in the enzyme assay than **29** (IC_{50} = 1.9 μM).

The early trend from our fragment data suggested that the carbon-linked malonate compounds in general bound more tightly than the oxygen-linked compounds and therefore had

dx.doi.org/10.1021/jm201734r | *J. Med. Chem.* 2012, 55, 3285−3306

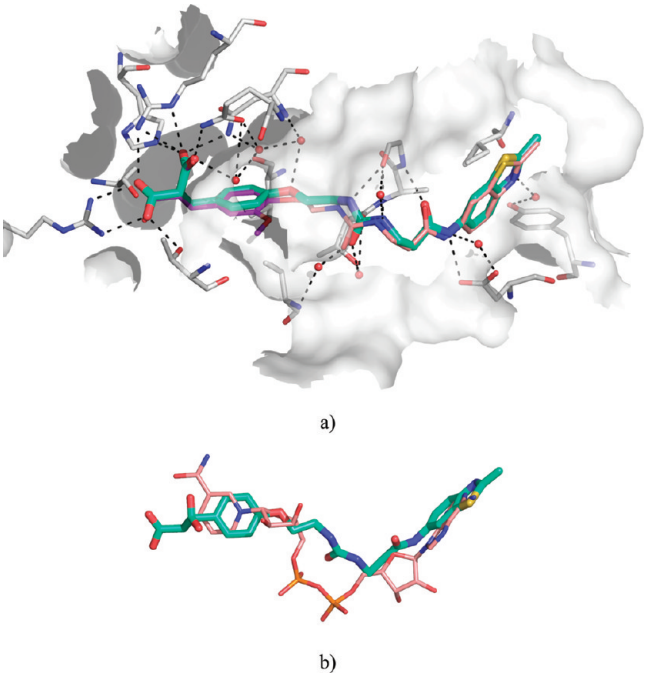

Figure 9. (a) X-ray crystal structure of **26** (cyan), overlaid with parent fragments (**21** and **24**, purple and pink, respectively). (b) X-ray crystal structure of **26** (cyan), overlaid with NADH as bound in 1i10[25] (pink). Protein and water atoms are omitted for clarity.

improved LE. This was also observed for the linked compounds. The carbon-linked versus oxygen-linked affinity was investigated in core 2. The O-linked compounds bound less tightly when comparing **29** (K_d = 0.069 μM) with **30** (1.2 μM) and **31** (K_d = 0.06 μM) with **32** (0.18 μM). This pattern was also observed in the enzyme activity of these compounds. In general, there is good agreement between the BIAcore binding data and enzyme assay for the linked compounds, with R^2 = 0.86 (Figure 10). Note that only linked compounds showing confirmed binding by BIAcore are included in Figure 10.

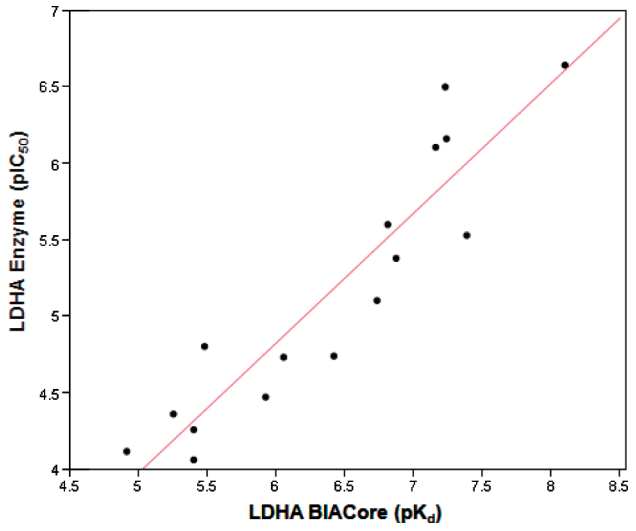

Figure 10. Correlation between BIAcore data (pK_d) and enzyme activity (pIC_{50}) for linked compounds. Line of best fit was calculated using least-squares regression.

A selection of compounds was tested in affinity-based LDHB assays.[64] Preliminary indications of selectivity over LDHB observed for some examples require further consolidation by testing with more physiologically relevant end points.

Examples of linked compounds with alternative cores (**29** and **33**) were soaked into the rat LDHA crystals and subsequently cocrystallized with human LDHA. They maintained a consistent overall binding mode as modeled, spanning the substrate, nicotinamide, and adenine pockets (Figure 11).

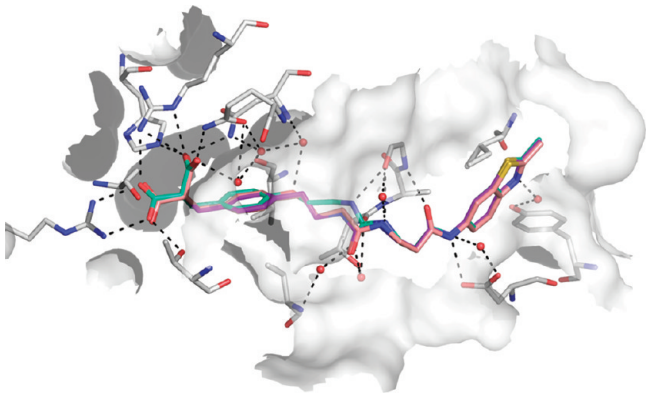

Figure 11. Binding mode of compounds **29** (purple) and **33** (pink) compared with **26** (cyan).

Comparison of the binding modes of **26**, **29**, and **33** to rat LDHA demonstrates the subtle effects on linker conformation resulting from alterations in the length and chemistry of the linker between the adenine and substrate binding site motifs. The linked compounds recapitulate the binding modes observed for the parent fragments, **21** and **24**; however, in order to accommodate the longer linker in **26**, the benzyl malonate of **26** is bound slightly deeper into the substrate pocket and rotated by ~8° with respect to that in **29** and **33**. An overlay of **26**, **29**, and **33** shows good agreement for the adenine and urea moieties, after which the path taken by the linker in **26** diverges from that of **29** and **33**. Electron density for this part of the linker region is consistent with a greater degree of torsional flexibility in **26** than in the shorter linkers of **29** and **33**. These binding modes were confirmed to be identical in human LDHA (Figure S5, Supporting Information), thus validating our exploitation of the more robust rat LDHA structural system as a surrogate.

Series Optimization. We had successfully designed novel LDHA inhibitors that bound tightly and showed potent enzyme activity in our assays. However, no cellular activity was seen for these compounds, which we assumed was due to the diacid moiety preventing cell penetration. To identify compounds with activity in cells, we synthesized and tested a set of mono- and diesters based on the diacid structures in Table 6. Some had already been made as precursors, while others were prepared by transesterification. We expected that this modification, which masks the acidic functionality, would allow the compounds to penetrate cell membranes. Subsequently, the cleavage of the esters into the active diacid form should occur once the compounds were inside the cell.[65] As we did not know what level of ester stability would be optimal, we synthesized both dimethyl and diethyl ester equivalents of the linked compounds, dimethyl esters being intrinsically less chemically stable than diethyl esters. Larger and more sterically hindered ester groups were considered to further modulate ester stability. However, the physical properties of these compounds would be expected to be poor. In order to achieve activity in cells the

dx.doi.org/10.1021/jm201734r | J. Med. Chem. 2012, 55, 3285−3306

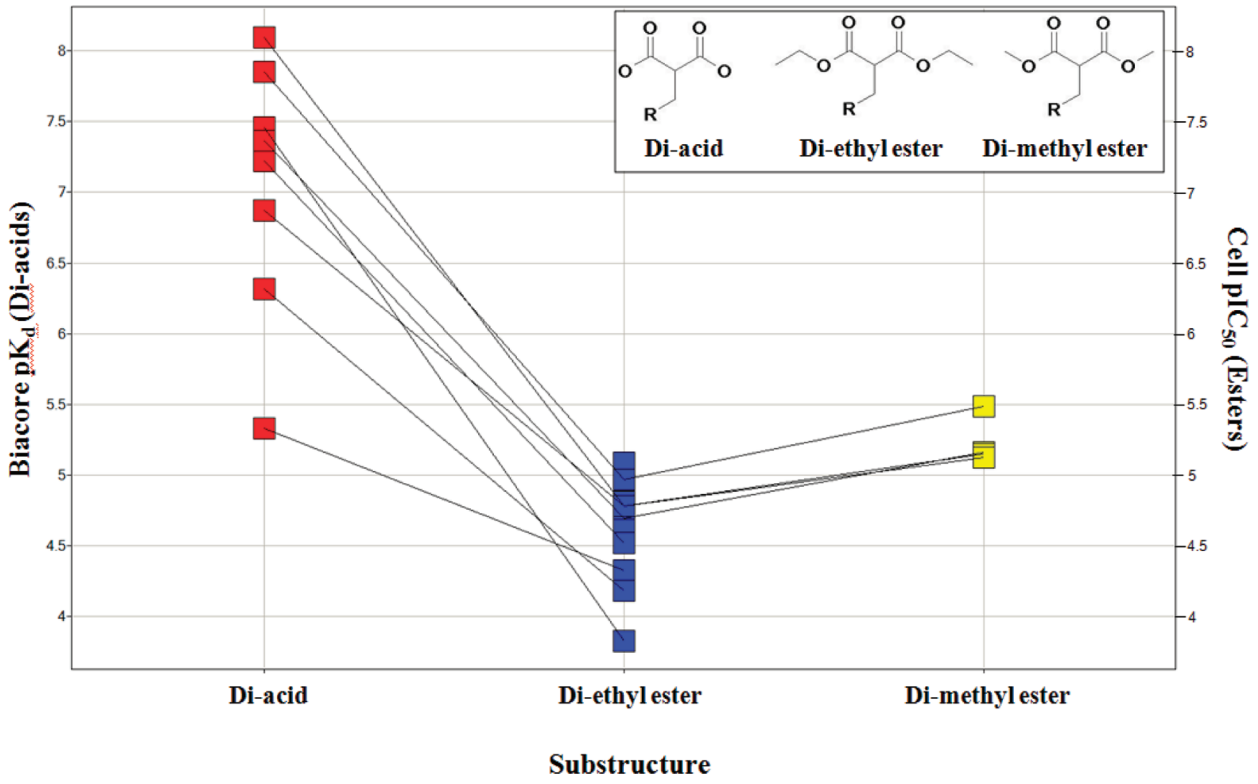

Figure 12. Binding affinity and cell activity comparison for carbon linked malonate diacids and diesters. The molecule substructure (diacid, diethyl, or dimethyl ester) is labeled on the *x*-axis. The *y*-axis shows the BIAcore binding pK_d for diacids and the cellular pIC_{50} for diesters. Data are the average of at least two experiments.

esters should cleave quickly once across the cell membrane; conversely, highly unstable esters may break down before entering the cell. This is particularly important when considering how these compounds may behave in more physiologically relevant environments. We assessed the cellular activity of compounds by measuring their effect on lactate levels in the culture media of SKBR3 cells. We did not see any consistent activity with monoesters. In contrast, cellular activity was observed with a range of diesters, the most potent of which had IC_{50} = 0.5 μM.

Figure 12 shows the BIAcore pK_d to cell pIC_{50} relationship for compounds that contain the carbon linked malonate group. Three different substructures are plotted across the *x*-axis: the diacid, the diethyl ester, and the dimethyl ester. On the *y*-axis are BIAcore pK_d data for the diacids or the cellular activity (pIC_{50}) if the compound is an ester. The lines indicate examples of these scaffolds where the acid-to-ester structural change is the only difference. This compound set shows a good BIAcore to cell relationship and improved cellular activity of the dimethyl ester when compared to the diethyl ester, which may be driven by the increased rate of ester hydrolysis.

We selected compound **35** (Scheme 12), among other diester examples, for further study as chemical probes. **35** was synthesized by transesterification of **71** with NaOMe; Knoevenagel reaction of aldehydes with dimethyl malonate gave almost exclusively bis-addition and was of no synthetic use. This specific compound had a reasonable combination of activity in cells (IC_{50} = 4.8 μM) and satisfactory overall physical properties. **35** is the dimethyl ester equivalent of compound **33**, which was one of the tightest binders synthesized with K_d = 0.093 μM by BIAcore and IC_{50}= 0.5 μM in our enzyme assay.

Scheme 12. Synthesis of Compound 35[a]

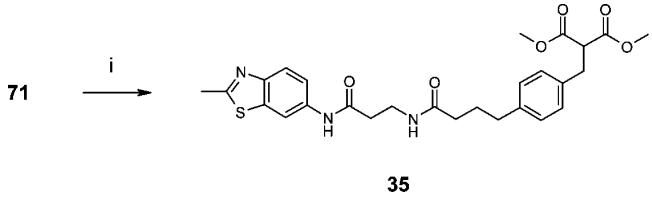

[a](i) NaOMe, MeOH, rt, 5 h, 90%.

CONCLUSIONS

We have reported on our FBLG approach against LDHA, which is an emerging target in cancer metabolism. Fragment-based approaches may prove to be a valuable way to identify inhibitors against this target, this thinking is further supported by Moses et al. recently publishing their work using a fragment approach.[81] As part of our strategy, we successfully identified fragments binding in the adenine and substrate regions of the active site. These fragments were then grown toward each other through iterative structure-based design and then linked to significantly increase potency while maintaining ligand efficiency, which has been shown to be a major challenge in the field of FBLG. The identified diacid lead compounds were converted into their respective esters at which point cellular activity was observed. To our knowledge these compounds represent the first potent LDHA inhibitors that have been fully validated through biophysical, enzymatic, and cellular assays along with binding mode elucidation by X-ray crystallography. Although these compounds require further optimization to deliver a compound suitable for in vivo experiments, such as modification/removal of the diacid functionality, the reported chemical equity presents significant progress toward this goal.

dx.doi.org/10.1021/jm201734r | J. Med. Chem. 2012, 55, 3285−3306

EXPERIMENTAL SECTION

X-ray Crystal Structures. Initial attempts to generate a soakable crystal system using human LDHA were unsuccessful. Although two different crystal forms of human LDHA were obtained, the active site loop in both of these was held in an open conformation by crystal contacts. Close inspection of the electron density revealed that the substrate site in these crystals was occupied by either citrate (from the crystallization buffer) or phosphate (from the purification buffer). In addition, the crystals were very fragile, grew under acidic conditions (pH 5.6), and diffracted to low resolution on an in-house source. Attempts to soak cofactor (NADH) plus oxamate or fragments into these crystals failed to yield complex crystal structures. Studies with rat LDHA yielded a more robust crystal system in which the active site loop adopted a closed conformation. These crystals grew under more neutral conditions (pH 7.0), diffracted to high resolution (>2 Å) on an in-house source, and were more amenable to soaking experiments. We hypothesized that the high sequence similarity of the NADH pockets would make the rat protein a suitable surrogate for human LDHA (Figure S1, Supporting Information). In the later stages of the project, extensive cocrystallization screening with a selection of more potent compounds yielded conditions under which cocrystals of human LDHA with linked compounds could be reliably produced, enabling us to confirm the validity of the rat system as a structural surrogate.

Crystals of rat LDHA(2−332) were grown at 293K by hanging-drop vapor diffusion by mixing purified protein at 20 mg/mL with a precipitant consisting of 1.3−1.5 M sodium malonate, pH 7.0, 2% glycerol in a 1:1 ratio to give a 4 μL drop. Drops were equilibrated overnight and then seeded using a 1:2500 dilution of freshly prepared seed stock (five crystals crushed in 10 μL of 1.6 M sodium malonate, pH 7.0). Crystals appear within 3 days and continue to grow for a further week. Complex structures were obtained by incubating these crystals for periods of 1−4 days in either citrate or malonate based soak buffer containing the compound of interest (2.5−10 mM) and ≤5% DMSO. Malonate based soak buffer (1.5 M sodium malonate, pH 7.0, 10% glycerol) was generally used for compounds predicted to bind at the adenine pocket, while citrate based soak buffer (1.3 M trisodium citrate, 0.04 M HEPES, pH 7.0, 10% glycerol) was used for compounds expected to bind at the substrate pocket. Crystals were then flash cooled in a gaseous nitrogen stream at 100 K prior to data collection. Rat LDHA(2−332) crystals belonged to the monoclinic space group $P2_1$ with unit cell dimensions of (62.1 ± 0.2) Å × (82.0 ± 0.5) Å × (129.1 ± 0.5) Å, β = (96.1 ± 0.1)°. The asymmetric unit comprises the biological tetramer.

Cocrystals of human LDHA(2−332)-6His with **33** were grown by incubating purified protein at 27 mg/mL with 2 mM **33** (2% DMSO) on ice for 30 min and then setting up a hanging-drop vapor diffusion experiment at 293 K using a 1:1 ratio of reservoir (0.1 M MES, pH 6.5, 1.6 M ammonium sulfate, 10% v/v 1,4-dioxane) to protein + compound to give a 2 μL drop. A narrow grid screen around these conditions was subsequently used successfully to generate cocrystal structures with several other compounds of similar chemotype. Crystals were cryoprotected by quickly passing through a solution containing 2.5 M ammonium sulfate, 0.1 M Tris-HCl, pH 6.5, 10% glycerol and flash cooled in a cryostream at 100 K prior to data collection. Cocrystals of human LDHA(2−332)-6His with **33** belonged to the monoclinic space group $P2_1$ with unit cell dimensions of 64.6 Å × 137.4 Å × 84.1 Å, β = 102.1°. The asymmetric unit comprises the biological tetramer.

Diffraction data were generally collected in-house using a Rigaku FRE equipped with Osmic optics and a Saturn944 CCD detector at 100 K. Data for the rat LDHA−**28** complex and the human LDHA−**36** structure were collected at the ESRF on beamlines ID23-EH1 and ID29, respectively. Data processing was carried out using d*TREK[66] or XDS[67] as implemented within autoPROC.[68] Data reduction and structure solution by molecular replacement (initially using PDB code 1i10[25] as a search model) were carried out using programs from the CCP4 suite.[69] Compounds were modeled into the electron density using Flynn (version 1.1.1, Openeye Scientific Software, Inc.). The protein−compound complex model was refined using Refmac[70] and Buster (version 2.9.4, Global Phasing Ltd.) with intermediate rounds of model building in Coot.[71] The quality of the models was monitored using MolProbity,[72] Procheck,[73−75] and Mogul.[76] The final structures have been deposited in the Protein Data Bank together with structure factors and detailed experimental conditions (see Table S1, Supporting Information for crystallographic statistics and PDB accession codes).

Additional Comments on Differences in Occupancy and Binding Mode for Different Compounds among the Four Chains of the LDHA Tetramer. Electron density for compounds **12** and **18** is best defined in chain B and less well-defined in the other three chains. For compound **14**, additional electron density consistent with binding of **14** at a crystal contact was also noted; however, the quality of the density was not sufficient to permit modeling of the compound at this site. For compound **20**, initial electron density for bound compound was visible bridging the nicotinamide and substrate pockets of all four chains of the tetramer in the crystal asymmetric unit; however, it was more clearly defined in chains B and C than A and D. Interestingly, in chains B and C the diacid portion of **20** binds in a manner identical to that observed for malonate alone, while in chains A and D, where the electron density for bound compound is poorer quality, the overlap is less consistent. This is particularly clear in chain A, where residual density consistent with bound malonate, **19** (∼30% occupancy), was present. A difference in conformation of the Gln-99 side chain among the four chains in the tetramer might provide an explanation. Steric restrictions constrain **20** to bind in an identical manner to all four chains, while malonate, being smaller, can adjust to the local environment. For compounds **20** and **22** dual soak, consistent with the results obtained for single soaks, compound **20** is only observed in two of the four molecules in the asymmetric unit (chains B and C), and in one of these (chain C) malonate is only partially displaced, so both malonate and **20** are modeled at partial occupancy. For compounds **21** and **22** dual soak, compound **21** is only observed in two of the four molecules in the asymmetric unit (chains B and C). For compound **26**, positive difference density was observed on the surface of the protein in the vicinity of the adenine pocket, consistent with binding of additional copies of compound **26** at partial occupancy. This density was best modeled as two alternative conformations of compound **26**. Although this density was present in all four copies of the LDHA monomer in the asymmetric unit, additional copies of compound **26** have only been modeled in chains A, B, and C where the density was strongest. We hypothesize that this additional surface binding is an artifact of the high concentrations (2.5 mM) and extended incubation times (72 h) used in the crystal soaking experiment, as superstoichiometirc binding was not observed by other techniques (BIAcore, ITC) or for other similar compounds (compounds **29** and **33**).

Nuclear Magnetic Resonance (NMR). Human LDHA(2−332)-6His protein for 1D NMR was expressed and purified from *E. coli* cells as described (methods S4, Supporting Information). For 1D (ligand-observed) NMR studies, samples were prepared in 50 mM sodium phosphate buffer, pH 7.0, 0.02% sodium azide. For 2D (protein-observed) NMR studies, LDHA was uniformly labeled with ^{15}N and ^{2}H by growth in D_2O-based minimal medium containing ^{15}N-ammonium chloride as the sole nitrogen source. Samples were prepared in a buffer containing 100 mM HEPES, pH 7.5, 2 mM TCEP, 0.02% sodium azide. For 1D studies, the concentration of LDHA was 40−48 μM monomer (10−12 μM tetramer), while for 2D studies, samples containing 100 μM monomer (25 μM tetramer) were used. NMR spectra were acquired on Bruker Avance 600 MHz spectrometers at 298 K, using a 5 mm triple-resonance HCN cryoprobe. Ligand binding was detected using WaterLOGSY[77] and $T_1\rho$-filtered[78] 1D experiments in combination with 2D $^{1}H-^{15}N$ TROSY-HSQC[79] experiments to provide binding-site and K_d information. NMR fragment screens were carried out using mixtures of six compounds at 200 or 400 μM (final) per compound. Active compounds in the mixtures were identified by comparison with 1D reference spectra, and specific binding was confirmed through addition of 1 mM NADH. Compounds whose binding signal (WaterLOGSY or $T_1\rho$-filtered) was appreciably reduced in the presence of NADH were considered bona fide hits.

dx.doi.org/10.1021/jm201734r | J. Med. Chem. 2012, 55, 3285−3306

Surface Plasmon Resonance (SPR). A BIAcore 3000 or a BIAcore S51 instrument (GE Healthcare) was used to detect binding interactions using a direct binding assay format. Prior to activation, the research grade CM5 chip surface was preconditioned using two 50 μL injections each of 10 mM HCl, 50 mM NaOH, 0.1% SDS, and 0.085% H_3PO_4 at a flow rate of 100 μL/min. LDHA was immobilized on the sensor surface using standard amine coupling This was achieved by activating the sensor surface using 7 min injections of a mixture of 11.5 mg/mL *N*-hydroxysuccinimide with 75 mg/mL 1-ethyl-3-(3-dimethylaminopropyl)carbodiimide hydrochloride. Protein immobilization was accomplished using a 10 min injection of hLDHA-6Lys-6His (500 μg/mL) or hLDHA(2−332)-6His (100 μg/mL) in 20 mM MES, pH 6.0 buffer. Remaining reactive esters were blocked using a 7 min injection of 1 M ethanolamine, pH 8.5, at a flow rate of 5 μL/min. Immobilization levels typically were around 15 000 resonance units. Reference flow cells were prepared without the protein, as well as with a denatured protein surface. Denaturation was achieved by a 30 s injection of 10 mM HCl at a flow rate of 30 μL/min. All binding measurements were performed in 20 mM Na phosphate, 150 mM NaCl, 0.005% v/v P20, 5% DMSO, pH 7.4, at a flow rate of 30 μL/min. Compounds were injected over the active protein and two reference surfaces with at least 30 s association and dissociation times. Solvent calibration and double referencing subtractions were made to eliminate refractive index change and injection noise using Scrubber 2.0 (BioLogic Software). Surface regeneration was achieved using dissociation for a time period allowing the response to return to baseline. Control injections of a fixed, saturating NADH concentration of 100 μM were interspersed with injections of compound to allow monitoring of the functionality of the protein surface. SPR equilibrium binding data, consisting of R_{eq} values from 8−10 point concentration series, were analyzed by fitting a simple 1:1 binding model to yield R_{max} and K_d values using Grafit 6 (Erithacus Software).

Biological Testing. *Compound Preparation.* Compounds were dispensed into black low volume 384-well plates (Griener Bio One, U.K., catalog no. 784076) using a Labcyte Echo 550 as previously described.[80] The test range was dependent on the stock concentration of compound but was typically across 12 points, using half log intervals with the exception of the last point which was a whole log interval from the 11th point. Each well was backfilled with the required volume of dimethyl sulfoxide (DMSO) to ensure a final DMSO concentration of 1% after addition of all reagents. In addition to the compound test wells each plate carried maximum and minimum controls. A compound known to inhibit LDHA was used as a maximum control. As a minimum control pure DMSO was added to wells.

Coupled Biochemical Enzyme Assay. After the addition of compounds to the assay plates 6 μL/well substrate solution was added followed by 6 μL/well enzyme solution. The substrate solution contained the following: 0.2 mM sodium pyruvate (Sigma, U.K., catalog no. P8574); 50 mM Tris, pH7.5; 50 mM KCl; 0.17% (v/v) Triton X100 (Sigma, U.K., catalog no. X100). The enzyme solution (comprising purified full length human recombinant LDHA at a working concentration of 0.012 μg/mL) contained 50 mM Tris, pH 7.5, 50 mM KCl, 0.17% (v/v) Triton X100, 0.06 mM NADH (Sigma, U.K., catalog no. N8129). The NADH solution was made fresh, as long-term storage can cause oxidation of the reduced reagent to NAD^+. Assay plates were incubated at room temperature (21 °C) for 60 min before the addition of 8 μL/well detection reagents. The detection reagent contained 5.03 U/mL diaphorase (Worthington Biochemcial Corp., NJ, U.S., catalog no. LS004330), 0.037 mM resazurin (Sigma, U.K., catalog no. R7017) made up in 50 mM Tris, pH 7.5, 50 mM KCl, 0.17% (v/v) Triton X100. Detection reagents were allowed to develop for 10 min before the plates were read using a Pherastar plate reader (BMG Labtech Ltd., U.K.). The reader required an excitation filter at a wavelength of 485 nm and emission filter at a wavelength of 540 nm.

Measurement of Cellular LDHA Activity. The SKBR3 cells were grown and passaged using RPMI 1640 (Sigma, R0883) medium supplemented with 20% fetal calf serum (FCS) and 1% (v/v) 200 mM L-glutamate (Invitrogen, catalog no. 25030-024). Prior to running the assay, cells were harvested and resuspended in a phenol red free RPMI 1640 (Sigma, catalog no. R7509) medium supplemented with 0.1% FCS and 1% (v/v) 200 mM L-glutamate. The cell number was estimated to be ∼1×10^5 cells per mL. Compounds or controls were dispensed into black clear-bottom tissue culture treated 384-well plates (Costar, catalog no. 3712) as previously described. After the addition of the compounds, 40 μL of cell suspension was added to each well and the plates were transferred to a standard tissue culture incubator for 4 h. Subsequently, 5 μL of culture medium was removed from each well into a second black 384-well plate. The level of lactate present in the 5 μL of culture medium was estimated using a lactate kit supplied by Trinity Biotech (catalog no. 735-10). To each well 30 μL of detection reagent was added, and plates were then stored in the dark for 10 min before reading absorbance at 450 nm using an Envision plate reader (Perkin-Elmer).

Calculation of IC_{50} Values. By use of the maximum and minimum control wells as references for the 0% and 100% enzyme inhibition points, it was possible to calculate the effect of each compound on the activity of the enzyme. OriginLab software was used to estimate the concentration of compound required to reduce the enzyme activity to 50%.

Chemistry. General Statements. ^{1}H NMR spectra were measured on a Bruker DPX-400 Ultrashield. Chemical shifts δ are reported relative to $CDCl_3$ at 7.26 ppm or DMSO-d_6 at 2.52 ppm as an internal standard. LC−MS spectra were obtained on a Waters 2790/ZMD LC−MS system equipped with a Waters 3100 mass spectrometer, a Waters Acquity photodiode array detector ranging from 200 to 320 nm, and a Phenomenex Gemini C18 110A column, 50 mm × 2.00 mm, with 5 μm silica, using a 5 min gradient of 5−95% MeCN in water. An amount of 0.1% (0.880 g/mL density) aqueous NH_3 was present as a basic modifier unless otherwise stated. All tested compounds were purified to >95% purity as determined by ^{1}H NMR and by HPLC total ion current over an array of wavelengths from 200 to 320 nm. NMR and mass spectra were run on isolated products and were consistent with the proposed structures. Normal phase column chromatography was performed on prepacked silica gel columns using an ISCO CombiFlash system.

Synthesis of Compounds 33 and 35. *Ethyl 4-Phenylbutanoate* ***65****.*[56] Sulfuric acid (4.0 mL, 122 mmol) was added to a solution of 4-phenylbutanoic acid (20.0 g, 122 mmol) in ethanol (150 mL) and the mixture heated at reflux for 20 h. The mixture was concentrated in vacuo and the residue dissolved in ethyl acetate (400 mL), washed with saturated $NaHCO_3$ solution (4 × 150 mL), brine (100 mL), dried over $MgSO_4$, and evaporated to dryness to afford ethyl 4-phenylbutanoate (23.11 g, 99%) as an orange liquid. ^{1}H NMR (400 MHz, $CDCl_3$, 30 °C) δ 1.25 (3H, t), 1.95 (1H, tt), 2.31 (2H, t), 2.65 (2H, t), 4.12 (2H, q), 7.16−7.21 (3H, m), 7.28 (2H, ddd).

Ethyl 4-(4-Formylphenyl)butanoate ***66****.* Hexamethylenetetramine (13.72 g, 97.84 mmol) was added to a solution of ethyl 4-phenylbutanoate **65** (17.1 g, 88.94 mmol) in TFA (88 mL) at 22 °C. The mixture was heated at 80 °C (internal temperature) under reflux for 16 h. The mixture was concentrated in vacuo and the residue partitioned between diethyl ether (150 mL) and saturated sodium hydrogen carbonate solution (100 mL). The aqueous layer was extracted with diethyl ether (3 × 100 mL), and the extracts were combined with the organic layer. The combined extracts were dried over $MgSO_4$ and evaporated to dryness. The residue was purified by flash silica chromatography. The elution solvent was 8% EtOAc in isohexane. Pure fractions were evaporated to dryness to afford ethyl 4-(4-formylphenyl)butanoate (6.11 g, 31.2%) as a colorless oil. ^{1}H NMR (400 MHz, $CDCl_3$, 30 °C) δ 1.26 (3H, t), 1.99 (2H, tt), 2.33 (2H, t), 2.74 (2H, t), 4.13 (2H, q), 7.35 (2H, d), 7.81 (2H, d), 9.98 (1H, s). HPLC t_R = 2.24 min.

4-(4-Formylphenyl)butanoic Acid ***67****.* Lithium hydroxide hydrate (4.17 g, 99.43 mmol) was added as a solution in water (100 mL) to a solution of ethyl 4-(4-formylphenyl)butanoate **66** (7.30 g, 33.14 mmol) in THF (100 mL) and ethanol (40 mL) at 22 °C, and the mixture was stirred for 16 h. The mixture was concentrated to a volume such that all of the organic solvent had been removed, diluted

with water (100 mL), and washed with diethyl ether (2 × 100 mL). The aqueous layer was acidified to pH 2 with 2 M HCl and extracted with ethyl acetate (3 × 150 mL). The combined extracts were washed with saturated brine (50 mL), dried over Na_2SO_4, and evaporated to afford impure 4-(4-formylphenyl)butanoic acid as a yellow solid. 4-(3-Carboxypropyl)benzoic acid was present as a 8% impurity (from air oxidation).

The impure solid was dissolved in DCM (200 mL) and sonicated. The resulting suspension was filtered, removing the white solid impurity 4-(3-carboxypropyl)benzoic acid (0.146 g). The filtrate was evaporated to afford 4-(4-formylphenyl)butanoic acid (5.81 g, 91%) as a pale yellow solid. ^{1}H NMR (400 MHz, DMSO-d_6, 30 °C) δ 1.84 (2H, tt), 2.24 (2H, t), 2.71 (2H, t), 7.44 (2H, d), 7.84 (2H, d), 9.98 (1H, s), 12.04 (1H, s). m/z (ES−), $(M - H)^-$ = 191.3; 5 min acidic method, HPLC t_R = 1.52 min.

Benzyl 4-(4-Formylphenyl)butanoate ***68***. 4-(4-Formylphenyl)-butanoic acid **67** (3.00 g, 15.61 mmol) was dissolved in DCM (200 mL), and 1*H*-imidazole (0.213 g, 3.12 mmol) and 1,1′-carbonyl diimidazole (3.04 g, 18.73 mmol) were added. The mixture was stirred at 22 °C for 3 h. Then benzyl alcohol (6.47 mL, 62.43 mmol) was added. The mixture was stirred at 22 °C for 16 h. The mixture was evaporated, and the residue was purified by flash silica chromatography. Elution gradient was 20% to 30% EtOAc in isohexane. Pure fractions were evaporated to dryness to afford benzyl 4-(4-formylphenyl)butanoate (3.57 g, 81%) as a colorless oil. ^{1}H NMR (400 MHz, $CDCl_3$, 30 °C) δ 2.01 (2H, tt), 2.39 (2H, t), 2.73 (2H, t), 5.12 (2H, s), 7.28−7.40 (7H, m), 7.79 (2H, d), 9.97 (1H, s). m/z (ES+), $(M + Na)^+$ = 305.5; 5 min acidic method, HPLC t_R = 2.68 min.

Diethyl 2-(4-(4-(Benzyloxy)-4-oxobutyl)benzylidene)malonate ***69***. A mixture of benzyl 4-(4-formylphenyl)butanoate **68** (500 mg, 1.77 mmol), diethyl malonate (0.296 mL, 1.95 mmol), PS-trisamine (purchased from Novabiochem, 100 mg, 0.42 mmol), and powdered activated 4 Å molecular sieves (200 mg) was suspended in toluene (20 mL). The mixture was heated at 50 °C for 16 h. Additional diethyl malonate (0.296 mL, 1.95 mmol), PS-trisamine (100 mg, 0.42 mmol), and powdered activated 4 Å molecular sieves (200 mg, 1.77 mmol) were added, and the mixture was stirred at 60 °C for a further 2 days. A 2:1 mixture of product/starting aldehyde was observed. The mixture was cooled to ambient temperature, filtered, and evaporated to dryness. The residue was purified by flash silica chromatography. Elution gradient was 15% to 25% EtOAc in isohexane. Complete separation was not achieved. Product-containing fractions were evaporated to afford a 83:17 mixture of diethyl 2-(4-(4-(benzyloxy)-4-oxobutyl)benzylidene)malonate (405 mg, 53.9%) and starting aldehyde **68**, as a colorless gum. ^{1}H NMR (400 MHz, $CDCl_3$, 30 °C) δ 1.29 (3H, t), 1.33 (3H, t), 1.98 (2H, tt), 2.37 (2H, t), 2.65 (2H, t), 4.30 (2H, q), 4.33 (2H, q), 5.11 (2H, s), 7.16 (2H, d), 7.37 (2H, d), 7.69 (1H, s). m/z (ES+), $(M + Na)^+$ = 447.2; 5 min acidic method, HPLC t_R = 3.21 min.

4-(4-(3-Ethoxy-2-(ethoxycarbonyl)-3-oxopropyl)phenyl)butanoic Acid ***70***. Impure diethyl 2-(4-(4-(benzyloxy)-4-oxobutyl)-benzylidene)malonate **69** (contaminated with aldehyde **68**, mixture contained 352 mg, 0.83 mmol of **69**) was dissolved in ethyl acetate (25 mL), and the mixture was degassed and purged with nitrogen. Then 5% palladium on carbon (70.6 mg, 0.03 mmol) was added and the mixture degassed and purged with hydrogen. The mixture was stirred under a balloon of hydrogen for 16 h. The mixture was degassed and purged with nitrogen, filtered, and evaporated to afford a 87:13 mixture of 4-(4-(3-ethoxy-2-(ethoxycarbonyl)-3-oxopropyl)phenyl)-butanoic acid and 4-*p*-tolylbutanoic acid (331 mg) as a colorless oil, which was carried through to the next stage without further purification. ^{1}H NMR (400 MHz, DMSO-d_6, 30 °C) δ 1.11 (6H, t), 1.72−1.81 (2H, m), 2.19 (2H, t), 2.51−2.59 (2H, m), 3.05 (2H, d), 3.78 (1H, t), 4.00−4.14 (4H, m), 7.07−7.15 (4H, m), 12.00 (1H, s). m/z (ES−), $(M - H)^-$ = 335.1; 5 min acidic method, HPLC t_R = 2.29 min.

2-(4-(4-(3-(2-Methylbenzo[d]thiazol-6-ylamino)-3-oxopropylamino)-4-oxobutyl)benzyl)malonate ***71***. HATU (275 mg, 0.72 mmol) was added dropwise as a solution in DMF (5 mL) to a solution of impure 4-(4-(3-ethoxy-2-(ethoxycarbonyl)-3-oxopropyl)phenyl)-butanoic acid **70** (contaminated with 4-(*p*-tolyl)butanoic acid; impure mixture contained 203 mg of **70**, 0.60 mmol), 3-amino-*N*-(2-methylbenzo[*d*]thiazol-6-yl)propanamide **49** (156 mg, 0.66 mmol), and DIPEA (0.137 mL, 0.78 mmol) in DMF (10 mL). The mixture was stirred at ambient temperature for 16 h. The mixture was evaporated and the residue partitioned between ethyl acetate (70 mL) and water (70 mL). The organic layer was washed sequentially with 0.1 M NH_4Cl solution (70 mL), water (2 × 70 mL), and saturated brine (30 mL), dried over Na_2SO_4, and evaporated. The residue was purified by flash silica chromatography, and elution gradient was 1−5% EtOH in DCM. Product-containing fractions were evaporated to dryness to afford 76% pure product as a colorless gum, contaminated with 23% *N*-(3-(2-methylbenzo[*d*]thiazol-6-ylamino)-3-oxopropyl)-4-*p*-tolylbutanamide. The crude product was stirred in diethyl ether for 16 h at 22 °C. The resulting white solid was collected by filtration, giving 85% pure material. This was crystallized from EtOAc/isohexane to give 92% pure material and recrystallized to give 95% pure diethyl 2-(4-(4-(3-(2-methylbenzo[*d*]thiazol-6-ylamino)-3-oxopropylamino)-4-oxobutyl)benzyl)malonate (202 mg, 60.5%) as a white crystalline solid. ^{1}H NMR (400 MHz, DMSO, 30 °C) δ 1.11 (6H, t), 1.68−1.82 (2H, m), 2.07 (2H, t), 2.48−2.60 (4H, m), 2.76 (3H, s), 3.03 (2H, d), 3.24−3.30 (2H, m), 3.36 (2H, dt), 3.75 (1H, t), 3.99−4.15 (4H, m), 6.98−7.15 (4H, m), 7.51 (1H, dd), 7.81 (1H, d), 7.89 (1H, t), 8.40 (1H, s), 10.11 (1H, s). m/z (ES+), $(M + H)^+$ = 554.3; 5 min acidic method, HPLC t_R = 2.25 min.

2-(4-(4-(3-(2-Methylbenzo[d]thiazol-6-ylamino)-3-oxopropylamino)-4-oxobutyl)benzyl)malonic Acid ***33***. Sodium hydroxide (11 mg, 0.27 mmol) was added as a solution in water (5 mL) to a solution of diethyl 2-(4-(4-(3-(2-methylbenzo[*d*]thiazol-6-ylamino)-3-oxopropylamino)-4-oxobutyl)benzyl)malonate **71** (38 mg, 0.07 mmol) in ethanol (5 mL) at 22 °C, and the mixture was stirred for 16 h, giving mostly monoacid. The mixture was concentrated to a volume such that all of the ethanol had been removed, diluted with water (5 mL), and stirred for a further 3 days at 22 °C. The mixture was diluted with water (20 mL) and washed with diethyl ether (20 mL). The aqueous layer was acidified to pH 2 with 2 M HCl and extracted with ethyl acetate (4 × 20 mL). The combined organics were washed with saturated brine (15 mL), dried over Na_2SO_4, evaporated and the residue was triturated with diethyl ether to afford 2-(4-(4-(3-(2-methylbenzo[*d*]thiazol-6-ylamino)-3-oxopropylamino)-4-oxobutyl)-benzyl)malonic acid (27 mg, 79%) as a white crystalline solid. ^{1}H NMR (400 MHz, DMSO, 30 °C) δ 1.77 (2H, tt), 2.07 (2H, t), 2.45−2.57 (4H, m), 2.76 (3H, s), 2.98 (2H, d), 3.36 (2H, dt), 3.52 (1H, t), 7.05 (2H, d), 7.09 (2H, d), 7.51 (1H, dd), 7.81 (1H, d), 7.89 (1H, t), 8.39 (1H, d), 10.11 (1H, s), 12.65 (2H, s). m/z (ES+), $(M + H)^+$ = 498.5; HPLC t_R = 1.65 min.

Dimethyl 2-(4-(4-(3-(2-Methylbenzo[d]thiazol-6-ylamino)-3-oxopropylamino)-4-oxobutyl)benzyl)malonate ***35***. Sodium metal (8.3 mg, 0.36 mmol) was added to methanol (10 mL), and the mixture was stirred until effervescence had ceased. Diethyl 2-(4-(4-(3-(2-methylbenzo[*d*]thiazol-6-ylamino)-3-oxopropylamino)-4-oxobutyl)benzyl)-malonate **33** (100 mg, 0.18 mmol) was added and the mixture stirred at 22 °C for 5 h. The mixture was quenched with saturated NH_4Cl solution (1 mL) and evaporated to a volume such that all of the methanol had been removed. The residue was partitioned between ethyl acetate (20 mL) and water (20 mL). The aqueous layer was extracted with ethyl acetate (2 × 20 mL), and the extracts were combined with the organic layer. The combined extracts were washed with saturated brine (20 mL), dried over Na_2SO_4, and evaporated to dryness. The residue was triturated with diethyl ether to afford dimethyl 2-(4-(4-(3-(2-methylbenzo[*d*]thiazol-6-ylamino)-3-oxopropylamino)-4-oxobutyl)benzyl)malonate (85 mg, 90%) as a white crystalline solid. ^{1}H NMR (400 MHz, DMSO, 30 °C) δ 1.68−1.83 (2H, m), 2.07 (2H, t), 2.45−2.57 (4H, m), 2.76 (3H, s), 3.04 (2H, d), 3.36 (2H, dt), 3.61 (6H, s), 3.80 (1H, t), 7.02−7.10 (4H, m), 7.51 (1H, dd), 7.81 (1H, d), 7.89 (1H, t), 8.40 (1H, d), 10.11 (1H, s). m/z (ES+), $(M + H)^+$ = 526.5; HPLC t_R = 2.00 min.

■ ASSOCIATED CONTENT

Supporting Information

Additional information on computational methodology, protein purification, sequence analyses, protein−ligand crystal structures, and compound synthesis. This material is available free of charge via the Internet at http://pubs.acs.org.

Accession Codes

[†]The following crystal structures have been deposited in the RCSB Protein Data Bank: codes 4aj1, 4aj2, 4aj4, 4aje, 4aji, 4ajk, 4ajh, 4ajj, 4ajl, 4al4, 4ajh, 4ajo, and 4ajp.

■ AUTHOR INFORMATION

Corresponding Author

*Phone: +44 (0)1625 519045. E-mail: richard.a.ward@astrazeneca.com.

Present Address

[‡]Merck KGaA, Frankfurter Strasse 250, D-64293 Darmstadt, Germany.

Notes

The authors declare no competing financial interest.

■ ACKNOWLEDGMENTS

The authors acknowledge Ann-Kathrin Schott, Isabelle Green, and Jon Read for construct design; Graham Sproat for molecular biology; Judith Stanway, Richard Ernill, and Linda MacCallum for protein expression; Ian Hardern for protein purification; Helen McMiken for crystallization screening and initial crystallization optimization experiments; Judit Debreczeni, Andrew Ferguson, Marie Fraser, and Joe Patel for structure refinements; the ESRF MXpress team for data collection; Chris De Savi, Ian Hollingsworth, Alice Hooper, Dave Perkins, Matt Addie, Matt Grist, Jo Allen, and Kelly-Marie Johnson for chemistry support; Nicky Whalley and Tom Dunkley for compound profiling; Martin Watson for SPR and NMR support; Clare Lane, Alison Hunter, and Kin Tam for pharmacokinetic (PK) and physical property assessment.

■ ABBREVIATIONS USED

LDH, lactate dehydrogenase; LDHA, lactate dehydrogenase A; LDHB, lactate dehydrogenase B; FBLG, fragment-based lead generation; NMR, nuclear magnetic resonance; SPR, surface plasmon resonance; HTS, high throughput screening; LE, ligand efficiency; LLE, ligand lipophilicity efficiency

■ REFERENCES

(1) Warburg, O. On the origin of cancer cells. *Science* **1956**, *123*, 309−314.

(2) Kim, J.; Dang, C. V. Cancer's molecular sweet tooth and the Warburg effect. *Cancer Res.* **2006**, *66*, 8927−8930.

(3) Zhuang, L.; Scolyer, R. A.; Murali, R.; McCarthy, S. W.; Zhang, X. D.; Thompson, J. F.; Hersey, P. Lactate dehydrogenase 5 expression in melanoma increases with disease progression and is associated with expression of Bcl-XL and Mcl-1, but not Bcl-2 proteins. *Mod. Pathol.* **2010**, *23*, 45−53.

(4) Koukourakis, M. I.; Giatromanolaki, A.; Winter, S.; Leek, R.; Sivridis, E.; Harris, A. L. Lactate dehydrogenase 5 expression in squamous cell head and neck cancer relates to prognosis following radical or postoperative radiotherapy. *Oncology* **2009**, *77*, 285−292.

(5) Kolev, Y.; Uetake, H.; Takagi, Y.; Sugihara, K. Lactate dehydrogenase-5 (LDH-5) expression in human gastric cancer: association with hypoxia-inducible factor (HIF-1alpha) pathway, angiogenic factors production and poor prognosis. *Ann. Surg. Oncol.* **2008**, *15*, 2336−2344.

(6) Koukourakis, M. I.; Giatromanolaki, A.; Sivridis, E.; Gatter, K. C.; Harris, A. L. Lactate dehydrogenase 5 expression in operable colorectal cancer: strong association with survival and activated vascular endothelial growth factor pathway—a report of the tumour angiogenesis research group. *J. Clin. Oncol.* **2006**, *24*, 4301−4308.

(7) Koukourakis, M. I.; Giatromanolaki, A.; Sivridis, E.; Bougioukas, G.; Didilis, V.; Gatter, K. C.; Harris, A. L. Lactate dehydrogenase-5 (LDH-5) overexpression in non-small-cell lung cancer tissues is linked to tumour hypoxia, angiogenic factor production and poor prognosis. *Br. J. Cancer* **2003**, *89*, 877−885.

(8) Le, A.; Cooper, C. R.; Gouw, A. M.; Dinavahi, R.; Maitra, A.; Deck, L. M.; Royer, R. E.; Vander Jagt, D. L.; Semenza, G. L.; Dang, C. V. Inhibition of lactate dehydrogenase A induces oxidative stress and inhibits tumor progression. *Proc. Natl. Acad. Sci. U.S.A.* **2010**, *107*, 2037−2042.

(9) Granchi, C.; Roy, S.; Giacomelli, C.; Macchia, M.; Tuccinardi, T.; Martinelli, A.; Lanza, M.; Betti, L.; Giannaccini, G.; Lucacchini, A.; Funel, N.; Leon, L. G.; Giovannetti, E.; Peters, G. J.; Palchaudhuri, R.; Calvaresi, E. C.; Hergenrother, P. J.; Minutolo, F. Discovery of *N*-hydroxyindole-based inhibitors of human lactate dehydrogenase isoform A (LDH-A) as starvation agents against cancer cells. *J. Med. Chem.* **2011**, *54*, 1599−1612.

(10) Javed, M. H.; Waqar, M. A. Effect of various metals and metabolites on the activity of lactate dehydrogenase. *Pak. J. Pharmacol.* **1993**, *10*, 7−14.

(11) Rees, D. C.; Congreve, M.; Murray, C. W.; Carr, R. Fragment-based lead discovery. *Nat. Rev. Drug Discovery* **2004**, *3*, 660−672.

(12) Albert, J. S.; Blomberg, N.; Breeze, A. L.; Brown, A. J. H.; Burrows, J. N.; Edwards, P. D.; Folmer, R. H. A.; Geschwindner, S.; Griffen, E. J.; Kenny, P. W.; Nowak, T.; Olsson, L.; Sanganee, H.; Shapiro, A. B. An integrated approach to fragment-based lead generation: philosophy, strategy and case studies from AstraZeneca's drug discovery programmes. *Curr. Top. Med. Chem. (Sharjah, United Arab Emirates)* **2007**, *7*, 1600−1629.

(13) Woodhead, A. J.; Angove, H.; Carr, M. G.; Chessari, G.; Congreve, M.; Coyle, J. E.; Cosme, J.; Graham, B.; Day, P. J.; Downham, R.; Fazal, L.; Feltell, R.; Figueroa, E.; Frederickson, M.; Lewis, J.; McMenamin, R.; Murray, C. W.; O'Brien, M. A.; Parra, L.; Patel, S.; Phillips, T.; Rees, D. C.; Rich, S.; Smith, D.; Trewartha, G.; Vinkovic, M.; Williams, B.; Woolford, A. J. Discovery of (2,4-dihydroxy-5-isopropylphenyl)-[5-(4-methylpiperazin-1-ylmethyl)-1,3-dihydroisoindol-2-yl]methanone (AT13387), a novel inhibitor of the molecular chaperone Hsp90 by fragment based drug design. *J. Med. Chem.* **2010**, *53*, 5956−5969.

(14) Huth, J. R.; Park, C.; Petros, A. M.; Kunzer, A. R.; Wendt, M. D.; Wang, X.; Lynch, C. L.; Mack, J. C.; Swift, K. M.; Judge, R. A.; Chen, J.; Richardson, P. L.; Jin, S.; Tahir, S. K.; Matayoshi, E. D.; Dorwin, S. A.; Ladror, U. S.; Severin, J. M.; Walter, K. A.; Bartley, D. M.; Fesik, S. W.; Elmore, S. W.; Hajduk, P. J. Discovery and design of novel HSP90 inhibitors using multiple fragment-based design strategies. *Chem. Biol. Drug Des.* **2007**, *70*, 1−12.

(15) Brough, P. A.; Barril, X.; Borgognoni, J.; Chene, P.; Davies, N. G. M.; Davis, B.; Drysdale, M. J.; Dymock, B.; Eccles, S. A.; Garcia-Echeverria, C.; Fromont, C.; Hayes, A.; Hubbard, R. E.; Jordan, A. M.; Jensen, M. R.; Massey, A.; Merrett, A.; Padfield, A.; Parsons, R.; Radimerski, T.; Raynaud, F. I.; Robertson, A.; Roughley, S. D.; Schoepfer, J.; Simmonite, H.; Sharp, S. Y.; Surgenor, A.; Valenti, M.; Walls, S.; Webb, P.; Wood, M.; Workman, P.; Wright, L. Combining hit identification strategies: fragment-based and in silico approaches to orally active 2-aminothieno[2,3-*d*]pyrimidine inhibitors of the Hsp90 molecular chaperone. *J. Med. Chem.* **2009**, *52*, 4794−4809.

(16) Barker, J. J.; Barker, O.; Boggio, R.; Chauhan, V.; Cheng, R. K. Y.; Corden, V.; Courtney, S. M.; Edwards, N.; Falque, V. M.; Fusar, F.; Gardiner, M.; Hamelin, E. M. N.; Hesterkamp, T.; Ichihara, O.; Jones, R. S.; Mather, O.; Mercurio, C.; Minucci, S.; Montalbetti, C. A. G. N.; Muller, A.; Patel, D.; Phillips, B. G.; Varasi, M.; Whittaker, M.; Winkler, D.; Yarnold, C. J. Fragment-based identification of Hsp90 inhibitors. *ChemMedChem* **2009**, *4*, 963−966.

(17) Cheng, Y.; Ashton, K.; Bartberger, M.; Brown, J.; Bryan, C.; Chen, K.; Esmay, J.; Fremeau, R. T.; Golden, J.; Harried, S.; Hickman, D.; Hitchcock, S. A.; Huang, M.; Jordan, B.; Judd, T.; Lopez, P.; Louie, S. W.; Luo, Y.; Mercede, S.; Michelsen, K.; Nixey, T.; Paras, N. A.; Poon, S.; Powers, T. S.; Sickmier, A.; St. Jean, D.; Tegley, C.; Zhong, W.; Wen, P.; Wahl, R. C.; Wood, S.; Xue, M.; Yang, B. From Fragment-Based Lead Generation to 2-Aminoquinolines as Potent beta-Secretase Inhibitors That Are Efficacious in Vivo. Presented at the 240th National Meeting of the American Chemical Society, Boston, MA, Aug 22−36, 2010; MEDI-288.

(18) Albert, J. S. Fragment-Based Lead Generation and Structure-Based Design for the Discovery of High Affinity Beta-Secretase Inhibitors. Presented at Frontiers in CNS and Oncology Medicinal Chemistry, ACS-EFMC, Siena, Italy, October 7−9, 2007; COMC-005.

(19) Albert, J. S. Discovery of High Affinity beta-Secretase Inhibitors Using Fragment-Based Lead Generation and Structure-Based Design. Presented at the 234th National Meeting of the American Chemical Society, Boston, MA, Aug 19−23, 2007; MEDI-243.

(20) Albert, J. S.; Edwards, P. D.; Andisik, D.; Campbell, J. B.; Congreve, M. S.; Carr, R.; Chessari, G.; Edfeldt, F.; Folmer, R. H. A.; Koether, G. M.; Kolmodin, K.; Murray, C. W.; Olsson, L.; Patel, S.; DeBeer, T. Fragment Based Lead Generation Approaches for Inhibitors of beta-Secretase: Development of a Novel Series of Isocytosine-Based Inhibitors. Presented at the 233rd National Meeting of the American Chemical Society, Chicago, IL, Mar 25−29, 2007; MEDI-311.

(21) Gill, A. New lead generation strategies for protein kinase inhibitors: fragment based screening approaches. *Mini-Rev. Med. Chem.* **2004**, *4*, 301−311.

(22) Tse, C.; Shoemaker, A. R.; Adickes, J.; Anderson, M. G.; Chen, J.; Jin, S.; Johnson, E. F.; Marsh, K. C.; Mitten, M. J.; Nimmer, P.; Roberts, L.; Tahir, S. K.; Xiao, Y.; Yang, X.; Zhang, H.; Fesik, S.; Rosenberg, S. H.; Elmore, S. W. ABT-263: a potent and orally bioavailable Bcl-2 family inhibitor. *Cancer Res.* **2008**, *68*, 3421−3428.

(23) Cunningham, B. T.; Laing, L. G. Advantages and application of label-free detection assays in drug screening. *Expert Opin. Drug Discovery* **2008**, *3*, 891−901.

(24) Bilitewski, U. Protein-sensing assay formats and devices. *Anal. Chim. Acta* **2006**, *568*, 232−247.

(25) Read, J. A.; Winter, V. J.; Eszes, C. M.; Sessions, R. B.; Brady, R. L. Structural basis for altered activity of M- and H-isozyme forms of human lactate dehydrogenase. *Proteins: Struct., Funct., Genet.* **2001**, *43*, 175−185.

(26) Smith, T. F.; Waterman, M. S.; Fitch, W. M. Comparative biosequence metrics. *J. Mol. Evol.* **1981**, *18*, 38−46.

(27) Edfeldt, F. N. B.; Folmer, R. H. A.; Breeze, A. L. Fragment screening to predict druggability (ligandability) and lead discovery success. *Drug Discovery Today* **2011**, *16*, 284−287.

(28) Cameron, A.; Read, J.; Tranter, R.; Winter, V. J.; Sessions, R. B.; Brady, R. L.; Vivas, L.; Easton, A.; Kendrick, H.; Croft, S. L.; Barros, D.; Lavandera, J. L.; Martin, J. J.; Risco, F.; Garcia-Ochoa, S.; Gamo, F. J.; Sanz, L.; Leon, L.; Ruiz, J. R.; Gabarro, R.; Mallo, A.; Gomez de las Heras, F. Identification and activity of a series of azole-based compounds with lactate dehydrogenase-directed anti-malarial activity. *J. Biol. Chem.* **2004**, *279*, 31429−31439.

(29) AstraZeneca, unpublished results.

(30) Sem, D. S.; Bertolaet, B.; Baker, B.; Chang, E.; Costache, A. D.; Coutts, S.; Dong, Q.; Hansen, M.; Hong, V.; Huang, X.; Jack, R. M.; Kho, R.; Lang, H.; Ma, C.; Meininger, D.; Pellecchia, M.; Pierre, F.; Villar, H.; Yu, L. Systems-based design of bi-ligand inhibitors of oxidoreductases filling the chemical proteomic toolbox. *Chem. Biol.* **2004**, *11*, 185−194.

(31) Baker, B. R.; Lee, W. W.; Skinner, W. A.; Martinez, A. P.; Tong, E. Potential anticancer agents—L. Non-classical antimetabolites. II. Some factors in the design of exoalkylating enzyme inhibitors, particulary of lactic dehydrogenase. *J. Med. Pharm. Chem.* **1960**, *2*, 633−657.

(32) Chapman, A. D. M.; Cortes, A.; Dafforn, T. R.; Clarke, A. R.; Brady, R. L. Structural basis of substrate specificity in malate dehydrogenases: crystal structure of a ternary complex of porcine cytoplasmic malate dehydrogenase, α-ketomalonate and tetrahydro-NAD. *J. Mol. Biol.* **1999**, *285*, 703−712.

(33) Blomberg, N.; Cosgrove, D. A.; Kenny, P. W.; Kolmodin, K. Design of compound libraries for fragment screening. *J. Comput.-Aided Mol. Des.* **2009**, *23*, 513−525.

(34) Hopkins, A. L.; Groom, C. R.; Alex, A. Ligand efficiency: a useful metric for lead selection. *Drug Discovery Today* **2004**, *9*, 430−431.

(35) DeLano, W. L. *The PyMOL Molecular Graphics System*; Schrodinger, LLC, 2003.

(36) Patel, J. U.; Prankerd, R. J.; Sloan, K. B. A prodrug approach to increasing the oral potency of a phenolic drug. 1. Synthesis, characterization, and stability of an *O*-(imidomethyl) derivative of 17β-estradiol. *J. Pharm. Sci.* **1994**, *83*, 1477−1481.

(37) Gubernator, K. (www.emolecules.com) The Comprehensive Source of Commercially Available, In Stock Chemicals. Presented at the 239th National Meeting of the American Chemical Society, San Francisco, CA, Mar 21−25, 2010; CINF-152.

(38) Cheng, A. C.; Coleman, R. G.; Smyth, K. T.; Cao, Q.; Soulard, P.; Caffrey, D. R.; Salzberg, A. C.; Huang, E. S. Structure-based maximal affinity model predicts small-molecule druggability. *Nat. Biotechnol.* **2007**, *25*, 71−75.

(39) Bembenek, S. D.; Tounge, B. A.; Reynolds, C. H. Ligand efficiency and fragment-based drug discovery. *Drug Discovery Today* **2009**, *14*, 278−283.

(40) Edwards, M. P.; Price, D. A. Role of physicochemical properties and ligand lipophilicity efficiency in addressing drug safety risks. *Annu. Rep. Med. Chem.* **2010**, *45*, 381−391.

(41) Orita, M.; Ohno, K.; Warizaya, M.; Amano, Y.; Niimi, T. Lead generation and examples opinion regarding how to follow up hits. *Methods Enzymol.* **2011**, *493*, 383−419.

(42) Karlberg, T.; Hammarstrom, M.; Schutz, P.; Svensson, L.; Schuler, H. Crystal structure of the catalytic domain of human PARP2 in complex with PARP inhibitor ABT-888. *Biochemistry* **2010**, *49*, 1056−1058.

(43) Woon, E. C. Y.; Threadgill, M. D. Poly(ADP-ribose)polymerase inhibition: Where now? *Curr. Med. Chem.* **2005**, *12*, 2373−2392.

(44) Chen, L.; Petrelli, R.; Felczak, K.; Gao, G.; Bonnac, L.; Yu, J. S.; Bennett, E. M.; Pankiewicz, K. W. Nicotinamide adenine dinucleotide based therapeutics. *Curr. Med. Chem.* **2008**, *15*, 650−670.

(45) Burgos, E. S.; Ho, M.; Almo, S. C.; Schramm, V. L. A phosphoenzyme mimic, overlapping catalytic sites and reaction coordinate motion for human NAMPT. *Proc. Natl. Acad. Sci. U.S.A.* **2009**, *106*, 13748−13753.

(46) Abad-Zapatero, C.; Griffith, J. P.; Sussman, J. L.; Rossmann, M. G. Refined crystal structure of dogfish M4 apo-lactate dehydrogenase. *J. Mol. Biol.* **1987**, *198*, 445−467.

(47) Dunn, C. R.; Wilks, H. M.; Halsall, D. J.; Atkinson, T.; Clarke, A. R.; Muirhead, H.; Holbrook, J. J. Design and synthesis of new enzymes based on the lactate dehydrogenase framework. *Philos. Trans. R. Soc. London, Ser. B* **1991**, *332*, 177−184.

(48) Hewitt, C. O.; Eszes, C. M.; Sessions, R. B.; Moreton, K. M.; Dafforn, T. R.; Takei, J.; Dempsey, C. E.; Clarke, A. R.; Holbrook, J. J. A general method for relieving substrate inhibition in lactate dehydrogenases. *Protein Eng.* **1999**, *12*, 491−496.

(49) Swiderek, K.; Panczakiewicz, A.; Bujacz, A.; Bujacz, G.; Paneth, P. Modeling of isotope effects on binding oxamate to lactic dehydrogenase. *J. Phys. Chem. B* **2009**, *113*, 12782−12789.

(50) Friesner, R. A.; Banks, J. L.; Murphy, R. B.; Halgren, T. A.; Klicic, J. J.; Mainz, D. T.; Repasky, M. P.; Knoll, E. H.; Shelley, M.; Perry, J. K.; Shaw, D. E.; Francis, P.; Shenkin, P. S. Glide: a new approach for rapid, accurate docking and scoring. 1. Method and assessment of docking accuracy. *J. Med. Chem.* **2004**, *47*, 1739−1749.

(51) Irvine, J. D.; Takahashi, L.; Lockhart, K.; Cheong, J.; Tolan, J. W.; Selick, H. E.; Grove, J. R. MDCK (Madin−Darby canine kidney) cells: a tool for membrane permeability screening. *J. Pharm. Sci.* **1999**, *88*, 28−33.

(52) Sidoova, E.; Odlerova, Z.; Volna, F.; Blockinger, G. Synthesis and antimicrobial activity of 2-alkylthio-6-aminobenzothiazoles. *Chem. Zvesti* **1979**, *33*, 830−836.
(53) Niederl, J. B.; Roth, R. T. Disproportionation in aryloxymalonic acid syntheses. *J. Am. Chem. Soc.* **1940**, *62*, 1154−1156.
(54) Krishnan, G. R.; Sreekumar, K. First example of organocatalysis by polystyrene-supported PAMAM dendrimers: highly efficient and reusable catalyst for Knoevenagel condensations. *Eur. J. Org. Chem.* **2008**, 4763−4768.
(55) Bigi, F.; Carloni, S.; Ferrari, L.; Maggi, R.; Mazzacani, A.; Sartori, G. Clean synthesis in water. Part 2. Uncatalysed condensation reaction of Meldrum's acid and aldehydes. *Tetrahedron Lett.* **2001**, *42*, 5203−5205.
(56) Bruno, I. J.; Cole, J. C.; Edgington, P. R.; Kessler, M.; Macrae, C. F.; McCabe, P.; Pearson, J.; Taylor, R. New software for searching the Cambridge Structural Database and visualizing crystal structures. *Acta Crystallogr., Sect. B: Struct. Sci.* **2002**, *58*, 389−397.
(57) Mauleon Casellas, D.; Carganico, G.; Fos Torro, M. D. L. D.; Garcia Perez, M. L.; Palomer Benet, A. Patent Application WO 9604267, 1996.
(58) Ichihara, O.; Barker, J.; Law, R. J.; Whittaker, M. Compound design by fragment-linking. *Mol. Inf.* **2011**, *30*, 298−306.
(59) Barker, J. J.; Barker, O.; Courtney, S. M.; Gardiner, M.; Hesterkamp, T.; Ichihara, O.; Mather, O.; Montalbetti, C. A. G. N.; Muller, A.; Varasi, M.; Whittaker, M.; Yarnold, C. J. Discovery of a novel Hsp90 inhibitor by fragment linking. *ChemMedChem* **2010**, *5*, 1697−1700.
(60) Hung, A. W.; Silvestre, H. L.; Wen, S.; Ciulli, A.; Blundell, T. L.; Abell, C. Application of fragment growing and fragment linking to the discovery of inhibitors of *Mycobacterium tuberculosis* pantothenate synthetase. *Angew. Chem., Int. Ed.* **2009**, *48*, 8452−8456.
(61) Bohacek, R. S. Computational Methods for Fragment Linking. Presented at the 236th National Meeting of the American Chemical Society, Philadelphia, PA, Aug 17−21, 2008; COMP-022.
(62) Fattori, D.; Squarcia, A.; Bartoli, S. Fragment-based approach to drug lead discovery: overview and advances in various techniques. *Drugs R&D* **2008**, *9*, 217−227.
(63) Crisman, T. J.; Bender, A.; Milik, M.; Jenkins, J. L.; Scheiber, J.; Sukuru, S. C. K.; Fejzo, J.; Hommel, U.; Davies, J. W.; Glick, M. "Virtual fragment linking": an approach to identify potent binders from low affinity fragment hits. *J. Med. Chem.* **2008**, *51*, 2481−2491.
(64) AstraZeneca, unpublished results.
(65) Beaumont, K.; Webster, R.; Gardner, I.; Dack, K. Design of ester prodrugs to enhance oral absorption of poorly permeable compounds: challenges to the discovery scientist. *Curr. Drug Metab.* **2003**, *4*, 461−485.
(66) Pflugrath, J. W. The finer things in X-ray diffraction data collection. *Acta Crystallogr., Sect. D: Biol. Crystallogr.* **1999**, *55*, 1718−1725.
(67) Kabsch, W. Software XDS for image rotation, recognition and crystal symmetry assignment. *Acta Crystallogr., Sect. D: Biol. Crystallogr.* **2010**, *66*, 125−132.
(68) Vonrhein, C.; Flensburg, C.; Keller, P.; Sharff, A.; Smart, O.; Paciorek, W.; Womack, T.; Bricogne, G. Data processing and analysis with the autoPROC toolbox. *Acta Crystallogr., Sect. D: Biol. Crystallogr.* **2011**, *67*, 293−302.
(69) Bailey, S. The CCP4 suite: programs for protein crystallography. *Acta Crystallogr., Sect. D: Biol. Crystallogr.* **1994**, *50*, 760−763.
(70) Murshudov, G. N.; Skubak, P.; Lebedev, A. A.; Pannu, N. S.; Steiner, R. A.; Nicholls, R. A.; Winn, M. D.; Long, F.; Vagin, A. A. REFMAC5 for the refinement of macromolecular crystal structures. *Acta Crystallogr., Sect. D: Biol. Crystallogr.* **2011**, *67*, 355−367.
(71) Emsley, P.; Cowtan, K. Coot: model-building tools for molecular graphics. *Acta Crystallogr., Sect. D: Biol. Crystallogr.* **2004**, *60*, 2126−2132.
(72) Chen, V. B.; Arendall, W. B. III; Headd, J. J.; Keedy, D. A.; Immormino, R. M.; Kapral, G. J.; Murray, L. W.; Richardson, J. S.; Richardson, D. C. MolProbity: all-atom structure validation for macromolecular crystallography. *Acta Crystallogr., Sect. D: Biol. Crystallogr.* **2010**, *66*, 12−21.
(73) Vaguine, A. A.; Richelle, J.; Wodak, S. J. SFCHECK: a unified set of procedures for evaluating the quality of macromolecular structure-factor data and their agreement with the atomic model. *Acta Crystallogr., Sect. D: Biol. Crystallogr.* **1999**, *55*, 191−205.
(74) Laskowski, R. A.; Rullmannn, J. A.; MacArthur, M. W.; Kaptein, R.; Thornton, J. M. AQUA and PROCHECK-NMR: programs for checking the quality of protein structures solved by NMR. *J. Biomol. NMR* **1996**, *8*, 477−486.
(75) Pontius, J.; Richelle, J.; Wodak, S. J. Deviations from standard atomic volumes as a quality measure for protein crystal structures. *J. Mol. Biol.* **1996**, *264*, 121−136.
(76) Allen, F. H. The Cambridge Structural Database: a quarter of a million crystal structures and rising. *Acta Crystallogr., Sect. B: Struct. Sci.* **2002**, *58*, 380−388.
(77) Dalvit, C.; Fogliatto, G.; Stewart, A.; Veronesi, M.; Stockman, B. WaterLOGSY as a method for primary NMR screening: practical aspects and range of applicability. *J. Biomol. NMR* **2001**, *21*, 349−359.
(78) Miyoshi, T. Slow dynamics of polymer crystallites revealed by solid-state MAS exchange NMR. *Kobunshi Ronbunshu* **2004**, *61*, 442−457.
(79) Zhu, G.; Xia, Y.; Nicholson, L. K.; Sze, K. H. Protein dynamics measurements by TROSY-based NMR experiments. *J. Magn. Reson.* **2000**, *143*, 423−426.
(80) Turmel, M.; Itkin, Z.; Liu, D.; Nie, D. An innovative way to create assay ready plates for concentration response testing using acoustic technology. *J. Lab. Autom.* **2010**, *15*, 297−305.
(81) Moorhouse, A. D.; Spiteri, C.; Sharm, P.; Zloh, M.; Moses, J. E. Targeting Glycolysis: a fragment based approach towards bifunctional inhibitors of hLDH-5. *Chem. Commun.* **2011**, *47*, 230−232.